

Spatial Stochastic Models of HSV-2 Lesion Dynamics and Their Link with HIV-1 Acquisition

by

Catherine Margaret M^cCombe Byrne

B.Sc. (Hons), Queen's University, 2013

A THESIS SUBMITTED IN PARTIAL FULFILLMENT OF
THE REQUIREMENTS FOR THE DEGREE OF

MASTER OF SCIENCE

in

THE FACULTY OF GRADUATE AND POSTDOCTORAL STUDIES

(Mathematics)

THE UNIVERSITY OF BRITISH COLUMBIA

(Vancouver)

July 2016

© Catherine Margaret M^cCombe Byrne 2016

Abstract

Patients with Herpes Simplex Virus-2 (HSV-2) infection face a significantly higher risk of contracting HIV-1. This marked increase is thought to be due not only to herpetic lesions serving as an entry point for the HIV-1 virus, but also to the increase in CD4+ T cells in the human genital mucosa during HSV-2 lesional events. By creating a stochastic, spatial, mathematical model describing the behaviour of the HSV-2 infection and immune response in the genital mucosa, I first capture the dynamics that occur during the development of an HSV-2 lesion. I then use this model to quantify the risk of acquiring HIV-1 in HSV-2 positive patients upon sexual exposure, and determine whether antivirals meant to control HSV-2 can decrease HIV-1 infectivity. While theory predicts that HSV-2 treatment should lower HIV-1 infection probability, my results show that this may not be the case unless a critical dosage of HSV-2 treatment is given to the patient. These results help to explain the conflicting data on HIV-1 infection probability in HSV-2 patients and allow for further insight into the type of treatment HSV-2 positive patients should receive to prevent HIV-1 infection.

Preface

All work presented in this dissertation is original, remains unpublished, and has been independently conducted by the author, Catherine Byrne.

Table of Contents

Abstract	ii
Preface	iii
Table of Contents	iv
List of Tables	vi
List of Figures	vii
Acknowledgements	ix
Dedication	x
1 Introduction	1
1.1 The Biology of a Genital HSV-2 Infection	1
1.2 The Link Between HSV-2 Lesional Events and HIV-1 Con- traction	2
1.3 Effects of HSV-2 Antiviral Drugs on HIV-1 Prevention	3
1.4 Goals	4
2 A Basic Model of HSV-2 Dynamics	5
2.1 Designing a Model of HSV-2 Infection in the Genital Mucosa	5
2.1.1 Adding Spatial Resolution to the Model Simulation Region	7
2.1.2 Defining Infection-Dependant Rates of Immune Cell Proliferation	9
2.2 Parameters of the Model	10
2.3 Simulations of HSV-2 Infection	12
2.3.1 Results of Model I for Immune Cell Proliferation	13
2.3.2 Results of Model II for Immune Cell Proliferation	20

Table of Contents

3	The Establishment of HSV-2 - HIV-1 Coinfection	26
3.1	A Description of HIV-1 Infection Dynamics	26
3.1.1	Defining HIV-1 Entry	27
3.1.2	Parameters for HIV-1	29
3.1.3	The Dynamics of HIV-1 Infection	29
3.2	Determining HIV-1 Infection Probability	33
4	Effects of HSV-2 Antivirals on HIV-1 Infection Probability	42
4.1	Impact of Antivirals on HSV-2 Infection and Lesion Development	42
4.2	Pritelivir's Impact on HIV-1 Infection Probability	46
4.2.1	HIV-1 Infection Probability for the Entire Genital Region	49
5	Conclusion	54
	Bibliography	57
 Appendix		
A	Main Python Code for HSV-2 Infection Simulations	63

List of Tables

2.1	Model parameter values for HSV-2 infection	12
3.1	Model parameter values for HIV-1 infection	29
3.2	Simulation scenarios used to find HIV-1 infection probabilities	35
3.3	Fold increases in per-coital HIV-1 risk when comparing expo- sure to chronic versus acute HIV-1 viral loads	40

List of Figures

2.1	Description of the model	8
2.2	HSV-2 infection dynamics with no spatial resolution	15
2.3	Summed HSV-2 infection dynamics on a 5×5 grid	16
2.4	Spatial HSV-2 infection dynamics on a 5×5 grid	17
2.5	Summed HSV-2 infection dynamics on a 15×15 grid	18
2.6	Spatial HSV-2 infection dynamics on a 15×15 grid	19
2.7	Summed HSV-2 infection dynamics on a 15×15 grid with the inclusion of cytokine effects	22
2.8	Spatial HSV-2 infection dynamics on a 15×15 grid with the inclusion of cytokine effects	23
2.9	Ten simulations of HSV-2 infection dynamics	25
3.1	Dynamics of HIV-1 infection establishment in an HSV-2 positive patient upon exposure to an acute dose of HIV-1 in the semen	31
3.2	Spatial dynamics of HIV-1 infection establishment	32
3.3	Per-coital act probability of HIV-1 infection in one simulation region upon exposure to HIV-1 from a chronically infected partner	36
3.4	Per-coital act probability of HIV-1 infection in one simulation region upon exposure to HIV-1 from an acutely infected partner	37
3.5	Probability of HIV-1 infection as dictated by CD4+ T cell count and damaged tissue amount	39
4.1	The effect of antivirals on lesion duration during HSV-2 infection	44
4.2	The effect of antivirals on lesional tissue damage during HSV-2 infection	45
4.3	The effect of antivirals on viral shedding during HSV-2 infection	45
4.4	The effect of antivirals on median HSV-2 infection traits	47
4.5	The effect of antivirals on median risk of HIV-1 contraction	48
4.6	Changing risk of HIV-1 over time for different antiviral doses	49

List of Figures

4.7	Probability of HIV-1 infection when considering all vaginal tissue	52
-----	--	----

Acknowledgements

Thank-you to Dr. Daniel Coombs for his guidance and support throughout the process of this thesis and to Rebeca Cardim-Falcão and Cole Zmurchok for their initial help in formulating the ideas of this research.

Dedication

To my family and to David who now knows more about herpes virus than I believe he ever wanted to.

Chapter 1

Introduction

Herpes Simplex Virus-2 (HSV-2) is one of the most common sexually transmitted infections (STIs) with an estimated 11.3% of the world's population being infected as of 2012 [26]. While the overall weakening of the immune system caused by some STIs often means that patients with STIs are coinfecting with other viruses, shockingly common is the establishment of HIV-1 in HSV-2 infected individuals. An estimated 38-60% of new HIV-1 infections in women and 8-49% of new HIV-1 infections in men may be attributed to previously established HSV-2 infections due to the optimal conditions a herpetic genital lesion presents for the entry and establishment of an invading HIV-1 virus [14, 20, 48]. As genital tissue becomes infected by HSV-2, large lesions can appear, damaging the natural barrier of the skin and providing entry points for the HIV-1 virus. In addition, the tissue surrounding a herpetic lesion is often rich in CD4+ immune cells, the main target cell for the HIV-1 virus. These conditions can cause a two to three-fold increase in the probability of HIV-1 virus infection establishment and drastically add to the spread of the HIV-1 epidemic [14, 30]. An increasing amount of research is being done to understand the relationship between HSV-2 and HIV-1 infections and to find ways to decrease the risk of HSV-2 positive patients acquiring an HIV-1 infection.

1.1 The Biology of a Genital HSV-2 Infection

HSV-2, the virus most commonly responsible for genital herpes, is thought to infect approximately 20 million people worldwide every year [26]. The spread of HSV-2 usually occurs through skin-to-skin genital contact where the virus enters the host through abrasions in the genital tract epithelium, infects an epithelial cell, and replicates. Following this initial infection, the virus spreads to nearby neurons where it establishes latency in the dorsal roots of the neural ganglions [40]. With the nervous system having very limited immune presence, this reservoir of HSV-2 in the neurons means a life-long infection for the host. A slow drip of virus from these neurons is released back into the genital tract where it may spark a new infection and

cause viral shedding [34].

The establishment and development of a herpetic lesion in the epithelial tissue is largely dependent on the immune presence at that site [34]. Despite the high number of shedding episodes that occur in HSV-2 positive patients, the immune system rapidly responds, clearing minor infection sites in two to twelve hours [15]. The two types of immune cells thought to be most important in HSV-2 infection control are the CD4+ and CD8+ T cells. Once the lesion is resolved, these immune cells also work to prevent re-infection, remaining at previous sites of infection for up to twenty weeks [36].

CD8+ T cells, which serve as cytotoxic cells for the immune system, are often thought of as the main force responsible for the control of HSV-2, both in neurons and in the infected epithelium [38]. As such, previous mathematical models of HSV-2 have included CD8+ T cells as the only immune cell present during HSV-2 infections [11, 34–37]. However, CD4+ T cells have more recently been shown to be important in the control of HSV. In experiments where CD8+ T cell deficient mice were infected with HSV-1, the virus and lesions could still be cleared at genital and neural sites. However, in the alternative situation where CD4+ T cell deficient mice were infected with HSV-1, the infection could not be cleared [23]. CD4+ T cells are thought to be the first cells to the site of infection and appear within the first 48 hours of HSV-2 infection in the epithelium [41]. Once CD4+ T cells arrive, they release interferon gamma (IFN- γ) and other cytokines causing CD8+ T cell recruitment to the infection site [28]. Activated CD8+ T cells then kill infected cells by delivering perforin and activating apoptotic pathways in the infected cell [9]. Further research on the role of CD4+ T cells in HSV-2 infections is essential to get a full understanding of HSV-2's pathobiology; similarly, CD4+ T cell dynamics should be included in mathematical models of the infection if we wish to obtain a full representation of the system.

1.2 The Link Between HSV-2 Lesional Events and HIV-1 Contraction

During an HSV-2 lesion, the presence of HSV-2 virus and infected epithelial cells cause stimulation and proliferation of immune cells which migrate to the lesion site. This influx of immune cells creates a favourable environment for an invading HIV-1 virus. Not only does the HIV-1 virus have a greater probability of successfully entering the body through the damaged tissue at the lesion site, but the immune response creates an environment dense in CD4+ T cells, the target cell of the HIV-1 virus [14, 43]. These CD4+ T

cells are also often enriched with chemokine receptor type 5 (CCR5), a co-receptor which HIV-1 commonly uses to enter its target cell [48]. This allows for easier and more frequent infection. The effect of HSV-2 infection on HIV-1 acquisition probability has also been shown through *ex-vivo* studies. When cervical tissue cultures infected with HSV-2 were exposed to HIV-1 virions, the virions bound more frequently to sites containing HSV-2 infected epithelial cells than to sites of healthy cells, directly showing that areas of HSV-2 infection are preferential sites for HIV-1 infection establishment [20].

HSV-2 coinfection with HIV-1 can also lead to higher transmission of HIV-1, with genital ulcers or microlesions shedding both HIV-1 and HSV-2 virus in coinfection scenarios [33]. With 80% of HSV-2 viral shedding events not coinciding with visible lesions, but instead to only small microlesions, this creates a potentially dangerous transmission scenario for both viruses [15]. Without proper knowledge about the state of their infection, infected individuals may remain asymptomatic and unknowingly pass on the HSV-2 or HIV-1 virus to sexual partners. Reciprocally, an asymptomatic HSV-2 positive individual may unknowingly be at an increased risk to invading viruses, including HIV-1, as they enter through the herpetic microlesions that are present. The synergy of these two viruses makes the scenario of coinfection dangerous and underscores the importance of preventing the establishment of the coinfection. An important avenue being explored for the control of these infections is the use of antiviral drugs.

1.3 Effects of HSV-2 Antiviral Drugs on HIV-1 Prevention

While no drug or vaccine has been developed that is capable of completely clearing or preventing HSV-2 infection, antivirals designed to decrease infection severity and outbreak frequency have long been available. Acyclovir and other related compounds work by inhibiting HSV-specific DNA polymerases [1]. By preventing HSV-2 replication, fewer virions are present to infect epithelial cells and initiate the development of herpetic lesions. Acyclovir has been shown to reduce the occurrence of genital lesions by 47-75% and the rate of viral shedding by 80% [8, 17].

These reductions in HSV-2 infection severity have promising implications for decreasing the rate of HIV-1 contraction. With fewer herpetic lesions, not only should there be less damaged tissue for the virus to enter through, but also fewer immune cells for the HIV-1 virus to infect. Despite this theory, studies on HIV-1 contraction risks present conflicting results. In

clinical studies observing HSV-2 positive individuals, the incidence of HIV-1 infection remained the same regardless of whether participants were or were not receiving acyclovir treatment [8, 18, 46]. While some have argued that antiviral doses may simply have not been high enough to observe a reduction in HIV-1 infection rates, the reason for this discrepancy is largely unknown [18]. Determining whether these antivirals can in fact decrease HIV-1 infection rates at a higher dosage would have important implications for the control of HIV-1 spread. The use of mathematical models can bring a better understanding of HSV-2 infection dynamics in patients receiving antivirals, and may help to determine correct dosage amounts.

1.4 Goals

While a considerable amount of mathematical modelling has been done to study HIV-1 or HSV-2 infections as they occur alone, [10, 11, 29, 31, 34–37, 39], none have analyzed the establishment of HIV-1 coinfection in individuals with chronic HSV-2 from a mechanistic and immunological perspective. Further, mathematical models have yet to be utilized to understand how HSV-2 antivirals may decrease the risk of HIV-1 contraction. Using a spatial stochastic model to describe the dynamics of a genital herpetic lesion caused by HSV-2, I quantify the risk of HIV-1 acquisition based on an individual's current state of HSV-2 infection. Further, I analyze the effect HSV-2 antiviral drugs may play in controlling HSV-2 outbreaks and inhibiting the establishment of HIV-1 infection, predicting dosage amounts needed for significant reductions in HIV-1 infection probability. This information has the potential to help both clinicians and patients understand when risks of HIV-1 acquisition are at their highest, and help guide doctors in choosing appropriate doses of HSV-2 antivirals to protect their patients against contracting HIV-1.

Chapter 2

A Basic Model of HSV-2 Dynamics

2.1 Designing a Model of HSV-2 Infection in the Genital Mucosa

To address questions related to viral dynamics at the site of herpetic lesions, I began by creating a mathematical model describing the basic dynamics occurring in the genital mucosa of an individual with a chronic HSV-2 infection. These dynamics, written as a system of ordinary differential equations (ODEs), are largely based on previous mathematical models of HSV-2 infections [11, 34–37], and are described in equations 2.1-2.5, tracking the number of healthy epithelial cells (H), infected epithelial cells (I), CD8+ T cells (E), CD4+ T cells (T), and HSV-2 virus (V) within the model.

$$\frac{dH}{dt} = g(H_0 - H) - \beta HV \quad (2.1)$$

$$\frac{dI}{dt} = \beta HV - fIE - aI \quad (2.2)$$

$$\frac{dE}{dt} = X_1 E - \delta E \quad (2.3)$$

$$\frac{dV}{dt} = \phi + pI - \beta HV - cV \quad (2.4)$$

$$\frac{dT}{dt} = \lambda + X_2 T - dT \quad (2.5)$$

The model is intended to describe a 2 cm \times 2 cm patch of epithelial cells within the genital epidermis of a chronically HSV-2 infected person. With herpetic lesions rarely reaching diameters greater than 6 mm, the 4 cm² surface area is meant to be large enough to contain any herpetic lesion that may occur at this site [34]. The simulation region has an assumed depth of 74 μ m, representing the average thickness of infectible epithelial tissue as measured by previous histological studies [34].

2.1. Designing a Model of HSV-2 Infection in the Genital Mucosa

H_0 represents the number of healthy epithelial cells present at the model site in the absence of infection. Taking the diameter of a healthy epithelial cell to be $17 \mu\text{m}$, and assuming a cuboidal cell shape, gives an H_0 of approximately 6×10^6 cells inside the model region [34]. The number of healthy epithelial cells either grows or shrinks proportional to how far H has strayed from H_0 at a rate constant g , capturing tissue repair mechanisms.

HSV-2 infections are initiated by the release of virus from neurons innervating the genital mucosa, which occurs at a constant rate ϕ . Healthy epithelial cells become infected by HSV-2 virus following the law of mass action at a rate proportional to β , and new virus is produced by these infected cells at a per-capita rate p . Free HSV-2 virus decays at a per-capita rate c . The presence of infected epithelial cells stimulates the proliferation of CD8+ T cells and CD4+ T cells in the genital mucosa at per-capita rates X_1 and X_2 respectively. X_1 and X_2 are assumed to be dependent on the state of the infection. Throughout the modelling process, X_1 and X_2 will take varying forms as described in subsection 2.1.2. Modelled CD8+ T cells are taken to be HSV-2 specific and interact and kill infected epithelial cells at a rate proportional to f , again following the law of mass action. Infected cells also die at a per-capita rate a as they succumb to the infection. CD8+ T cells leave the system at a per-capita rate δ , chosen to be low, representing the long period these cells remain at, and protect, previous sites of infection [23, 48]. In the infection-free state, a population of CD4+ T cells remain at the site, existing at an equilibrium number of λ/d . CD4+ T cells have not been included in previous models of HSV-2 infection [11, 34–37]. I include their dynamics due to their importance in the establishment of HIV-1 infections, which I analyze later, and in order to get a better representation of the full dynamics occurring at herpes lesion sites.

While this system of ODEs serves as a useful framework to write down the dynamics that are occurring in a herpetic lesion, their constant rates do not provide a good representation of what is occurring biologically during a lesion event. Solutions to a system of ODEs report smooth, average behaviours over time; however, the dynamics of a herpes infection show little resemblance to an average [34]. Instead, dynamics show fast, apparently random spikes of infection, followed often by equally fast clearance [34]. As such, I transferred the dynamics into a better suited stochastic framework, designing a chemical master equation to describe the system and the probability of different states. Using this chemical master equation, I implemented the Gillespie algorithm to simulate the progression of the system through time.

In the traditional Gillespie algorithm, the system progresses through

small time intervals, randomly chosen, during which one reaction is allowed to occur. Both the size of the time interval and reaction choice are made dependent on the probability of different events occurring within the system [12]. While previous mathematical models of herpes infections have been analyzed in a stochastic framework, none to my knowledge have used the true Gillespie algorithm, instead progressing the system through small, constant time steps and allowing reactions to occur with probabilities taken from known parameter distributions [11, 34–37]. While the Gillespie algorithm can be computationally expensive if reaction rates are fast, it is exact and better describes the behaviour of a system.

2.1.1 Adding Spatial Resolution to the Model Simulation Region

While knowing the overall dynamics occurring within the simulation region is useful, it would be helpful to have a clear idea about how a single lesion spatially develops. To gain a more specific representation of where reaction events take place, I added a spatial component to the Gillespie algorithm, placing the modelled region on a grid. The surface is divided into $n \times n$ equally sized sites, with each spanning the depth of the simulation region. This design allows the dynamics within each grid site to be tracked as the model runs. While the system still progresses through the Gillespie algorithm in much the same fashion, I now assume reactions only occur between cells and virions that exist within the same grid site. Since immune cells actively move around the epithelium in search of infection and viruses diffuse through their environment, I allow HSV-2 virus, CD4+ T cells, and CD8+ T cells to diffuse horizontally through the tissue into neighbouring grid sites. I define the rate of diffusion for a specific diffusing body $N \in \{E, T, V\}$ at grid site (i, j) , where $i, j \in \{1, 2, \dots, n\}$, as

$$D_{N_{i,j}} = \omega_N \frac{N_{i,j-1} + N_{i-1,j} - 4N_{i,j} + N_{i+1,j} + N_{i,j+1}}{h^2}. \quad (2.6)$$

Here, ω_N represents the diffusion coefficient specific to the diffusing body and h^2 represents the horizontal cross sectional area of each grid site.

At the boundaries of the simulation region, virus, CD8+ T cells, and CD4+ T cells can diffuse out of the system; however, as surrounding tissue also has immune presence, I allow CD8+ and CD4+ T cells to diffuse into the system from the borders. By allowing E_{ave} and T_{ave} to represent the average CD8+ T cell concentrations expected to exist in chronic HSV-2 infected tissue per simulation region, E_{ave}/n^2 and T_{ave}/n^2 represent the

2.1. Designing a Model of HSV-2 Infection in the Genital Mucosa

average CD8+ and CD4+ T cell concentrations per grid site on an $n \times n$ grid. Diffusion of CD8+ T cells and CD4+ T cells therefore occurs at rates $\omega_E E_{ave}/n^2$ and $\omega_T T_{ave}/n^2$ respectively. Virus is not allowed to enter from the boundary as I assume no other lesions are in close proximity to the modelled patch. A summary of this new model system is described in figure 2.1 while a description of the parameter values appears in Section 2.2.

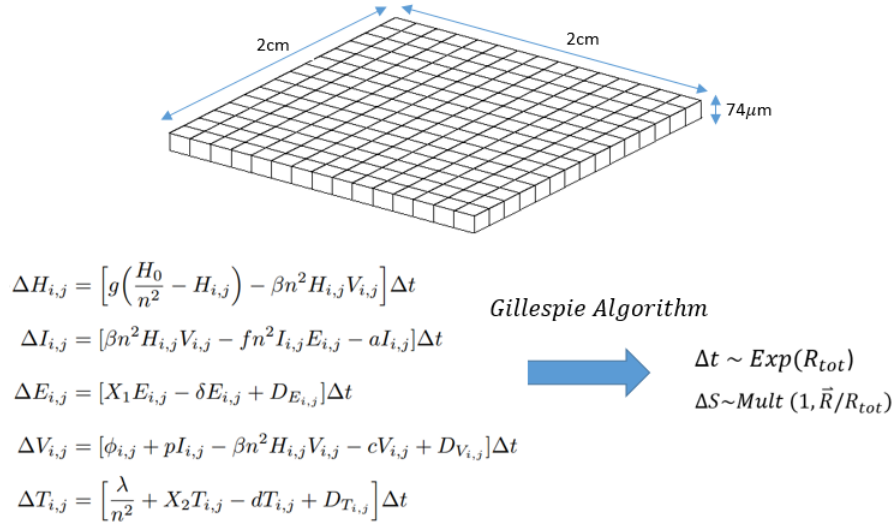


Figure 2.1: Description of the model. The ODE system presented in equations 2.1-2.5 is put into a spatial stochastic framework to capture the random events that occur during a herpes infection. The system progresses through small time steps (Δt) following an exponential distribution with rate R_{tot} equal to the sum of vector \vec{R} which contains all reaction rates in the system. During each time step, the system updates with one event (ΔS) being allowed to occur, chosen from a multinomial distribution where the probability of each event equals its rate of occurrence divided by R_{tot} . To gain further resolution on where reactions are occurring, the system is divided into $n \times n$ equally sized grid sites so that I can track the location of reactions and the dynamics occurring at every grid site (i, j) , where $i, j \in \{1, 2, \dots, n\}$. In addition to the dynamics described in the system of ODEs, HSV-2 virus, CD4+ T cells and CD8+ T cells are allowed to diffuse into neighbouring sites while infected and healthy epithelial cells are assumed to remain stationary. With n^2 grid sites per simulation region, parameters dependent on space were either divided or multiplied by n^2 to allow for the correct unit conversion.

2.1.2 Defining Infection-Dependant Rates of Immune Cell Proliferation

Model I: Immune Stimulation by Infected Cells

In determining the best representation of immune stimulation, I began with the simplest model, making X_1 and X_2 , the terms describing CD8+ and CD4+ T cell stimulation respectively, saturating functions dependent on the number of infected epithelial cells.

$$X_1 = \frac{I_{i,j}}{I_{i,j} + r_1/n^2} \theta_1 \quad (2.7)$$

$$X_2 = \frac{I_{i,j}}{I_{i,j} + r_2/n^2} \theta_2 \quad (2.8)$$

Here, $\theta_{1,2}$ is the maximum per-capita proliferation rate of immune cells, and $r_{1,2}$ is the number of infected cells needed to achieve half this proliferation rate within the entire simulation region. 1, 2 correspond to CD8+ stimulation and CD4+ stimulation respectively. To scale parameters to be specific to the size of a grid site, r_1 and r_2 are divided by n^2 .

While this representation of immune stimulation is functional in representing infection-dependent immune cell proliferation, it remains a simplification of the true biological system. Cytokines, small signalling molecules produced in response to infection, are the true components regulating and stimulating immune cell proliferation [28, 41]. As such, I develop a second, more complex model of the HSV-2 infection system, including the presence of cytokines and their effects on immune cell proliferation.

Model II: Including The Effects of Cytokines on Immune Stimulation

To capture the effects of cytokines on the immune response to HSV-2 infection within the genital mucosa, I define cytokine dynamics (C) at site (i, j) as follows:

$$\Delta C_{i,j} = [bI_{i,j} - mC_{i,j} + D_{C_{i,j}}] \Delta t, \quad (2.9)$$

where

$$D_{C_{i,j}} = \omega_C \frac{C_{i,j-1} + C_{i-1,j} - 4C_{i,j} + C_{i+1,j} + C_{i,j+1}}{h^2}. \quad (2.10)$$

2.2. Parameters of the Model

Cytokines are assumed to be produced at a rate b , dependent on the number of infected epithelial cells in the same grid site, and decay from the system at a per-capita rate m . I also assume they may diffuse into neighbouring grid sites with diffusion coefficient ω_C . These dynamics are transferred into the chemical master equation describing the system as a whole and changes in cytokine numbers occur through the Gillespie algorithm.

Rates of immune cell proliferation at site (i, j) are then made to be dependent on the number of cytokines at that site.

$$X_1 = \frac{C_{i,j}}{C_{i,j} + r_3/n^2} \theta_1, \quad (2.11)$$

$$X_2 = \frac{C_{i,j}}{C_{i,j} + r_4/n^2} \theta_2. \quad (2.12)$$

Again, I choose to use a saturating function to describe the rate at which cytokines stimulate immune cell production, with r_3 and r_4 now representing the number of cytokines needed to cause half the maximum proliferation rate of CD8+ and CD4+ T cells, respectively, in the entire simulation region. By including the dynamics of cytokines, in particular their ability to diffuse into neighbouring grid sites, the immune response to infection may show very different results to those predicted through the use of **Model I**.

2.2 Parameters of the Model

Due to recent interest in mathematically analyzing HSV-2 infections in the genital mucosa, many of the dynamics describing HSV-2 infection are well parameterized [11, 34–37]. However, my inclusion of CD4+ T cell dynamics at the lesion site has not previously been examined from a mathematical standpoint. I therefore determined new values for the parameters governing CD4+ T cell behaviour in the genital epithelium. One challenge surrounding this task was the limitation in data reporting CD4+ T cell numbers in the genital mucosa; however, as CD4+ T cells are the main target of the HIV-1 virus, a representation of their dynamics is essential if we want to address questions related to HIV-1 infection. Fortunately, recent studies on the immune presence in the genital mucosa during different stages of herpetic lesion development reported both CD4+ and CD8+ T cell numbers at the lesion sites [24, 48]. Using this data, I determined values for the undefined parameters.

A healthy individual without HSV-2 infection has approximately 68 CD4+ T cells per mm^2 circulating around the epidermal layer of the genital epithelium [48]. Scaling this number to the 4 cm^2 of my model region

2.2. Parameters of the Model

indicates there should be 27200 CD4+ cells in the model when the patient is infection-free, directly corresponding to the fraction λ/d . Assuming the death rate, d , of CD4+ T cells is similar to that of CD8+ T cells, I set $d = 0.07/\text{day}$ and $\lambda = 1900/\text{region-day}$ to achieve the correct infection-free equilibrium value. With these two parameter values chosen, the parameters found in the expression for X_2 , the rate of CD4+ T cell response to infection, remained to define. One common way of fitting mathematical models to data is to adjust the parameters of the model until the ODE solution curve matches the experimental data curve. However, this process is not as straightforward in the case of HSV-2 lesional events. As previously stated, the curves predicted by the ODE model are smooth averages of the system and have little resemblance to the stochastic nature of HSV-2 infection dynamics. Furthermore, lesion events within a patch of epithelium are relatively rare. It therefore makes little sense to fit a curve representing the average to data representing rare events. Instead, I used the closely linked dynamics of CD4+ and CD8+ T cells to determine parameters values governing X_2 . A striking feature appearing in the data is the relatively unchanging ratio between CD4+ and CD8+ T cells [24, 48]. During the progression of an HSV-2 genital lesion, the CD4+ to CD8+ T cell ratio remains fairly constant, ranging from approximately 0.6 to 2.0 with a mean value of 1.06 in healthy tissue and 1.24 in HSV-infected tissue [24, 48]. As parameters describing CD8+ T cell dynamics are already well known, I simply varied the parameters describing X_2 until I reached a state where the CD4+ to CD8+ T cell ratio consistently fell within an appropriate range. In running fifty, one-year simulations of the full model including cytokines, with parameters of $r_3 = 42/\text{day}$, $r_4 = 38/\text{day}$, $\theta_1 = 1.70/\text{day}$, and $\theta_2 = 1.40/\text{day}$, the CD4+ to CD8+ ratio had an average of 1.4, ranging from 0.7-3.1. With these ratios similar to those observed experimentally, these values were assumed acceptable for all remaining simulations.

Due to the division of the simulation region into specific grid sites during the spatial analysis of the model, those parameters dependent on space needed to be scaled accordingly. With n^2 grid sites per simulation region, parameters dependent on space were either divided or multiplied by n^2 to allow for the correct unit conversion. All parameter values of the model are recorded in table 2.1.

2.3. Simulations of HSV-2 Infection

Table 2.1: List of parameter values used in the model. Most parameter values were chosen to fall within the range of those found in the literature. Parameters without previously recorded values were estimated so that the model showed the correct, expected dynamics. Parameter time units are in terms of days, while those dependent on space are scaled to be in terms of one $2 \text{ cm} \times 2 \text{ cm} \times 74 \text{ }\mu\text{m}$ simulation region.

	Units	Value Chosen	Range in Literature			Citation
g	/day	0.22	0.22			[35]
β	region/day	1.0×10^{-7}	2.7×10^{-9}	–	6.6×10^{-7}	[11, 34–37]
a	/day	1.20	1.20	–	1.33	[34, 35]
f	region/day	0.010	0.001	–	0.200	[34, 35]
r_1	/region	42	5	–	200	[11, 34–37]
r_2	/region	38		–		–
r_3	/region	42		–		–
r_4	/region	38		–		–
θ_1	/day	1.70	0.98	–	7.20	[11, 34–37]
θ_2	/day	1.40		–		–
δ	/day	0.05	6.64×10^{-4}	–	8.30×10^{-2}	[11, 34–37]
p	/day	7.05×10^3	10^3	–	10^5	[11, 34–37]
c	/day	8.8	6.2	–	96.0	[11, 34–37, 42]
ϕ	/region-day	50	1	–	2000	[11, 34–37]
λ	/region-day	1900		–		–
d	/day	0.07		–		–
ω_V	cm^2/day	7.2×10^{-4}	2.8×10^{-6}	–	3.1×10^{-3}	[5, 25, 27]
ω_E, ω_T	cm^2/day	7.2×10^{-4}	1.3×10^{-4}	–	1.4×10^{-3}	[2, 4]
ω_C	cm^2/day	2.45×10^{-2}	1.30×10^{-2}	–	8.64×10^{-1}	[16, 21]
m	/day	6.2	2.8	–	6.6	[21, 45]
b	/day	24.8		–		–
n	–	5, 15		–		–
E_{ave}	/region	60,000		60,000		[34]
T_{ave}	/region	50,000		50,000		[48]
H_0	/region	6×10^6		6×10^6		[34]

With the model now fully developed, I move on to determine the effects of different spatial resolutions of the model and find which resolution presents the clearest representation of lesion development in the genital mucosa.

2.3 Simulations of HSV-2 Infection

A simulation begins with the modelled epithelial patch being lesion and virus-free, but still displaying the characteristics of chronic HSV-2 infection. The initial number of healthy epithelial cells is set to equal H_0 and the HSV-2 and infected cell counts are both zero. As immune cells have a prolonged presence at the sites of previous HSV-2 infection, the initial numbers of CD4+ and CD8+ T cells are not set to zero, but to numbers indicative

2.3. Simulations of HSV-2 Infection

of recently healed tissue with $E(0) = 60,000$ cells and $T(0) = 50,000$ cells [34]. The $2\text{ cm} \times 2\text{ cm}$ simulation region is assumed to be centered around an HSV-2 infected nerve, with virus being released into the central grid site at rate ϕ . To explore the effects of different definitions for immune stimulation rates, I first allowed proliferation rates to be dependent on infected cell counts, as described in **Model I** for immune cell proliferation, and later examined the effects of cytokine-dependent immune cell proliferation as described in **Model II**.

2.3.1 Results of Model I for Immune Cell Proliferation

Model simulations with X_1 and X_2 as described in equations 2.7 and 2.8, and with spatial resolutions of 1, 25, and 225 grid sites per simulation region, are reported in figures 2.2-2.6. Figures 2.2, 2.3, and 2.5 present HSV-2, infected cell, and immune cell counts summed across the entire simulation region over two months of infection. Figures 2.4 and 2.6 present spatially-specific data for model regions divided into 25 and 225 grid squares, showing HSV-2 counts, CD8+ T cell counts, and amounts of damaged tissue at each grid site during key times of lesion development. Here, tissue damage at site (i, j) is reported as the fraction of epithelial cells missing from a grid site and contributing to the lesion. This value is defined as

$$L_{i,j} = \frac{H_0/n^2 - H_{i,j} - I_{i,j}}{H_0/n^2}, \quad (2.13)$$

with H_0/n^2 being the expected number of healthy epithelial cells at a grid site in the absence of infection. This formula can also be modified to find the fraction of tissue damage within the entire simulation region:

$$L_{\text{tot}} = \frac{H_0 - \sum_{\forall i} \sum_{\forall j} H_{i,j} - \sum_{\forall i} \sum_{\forall j} I_{i,j}}{H_0}. \quad (2.14)$$

Regardless of the spatial resolution, each simulation captured the stochastic dynamics that appear during herpetic lesions. Viral peaks in the simulations varied in size, corresponding to different severities of outbreaks, and matching with those recorded in the literature [34, 48].

On examination of the spatially resolved information collected during the simulations, one can note a large difference in the visualization of lesion development when the simulation region is divided into 25 versus 225 grid squares. While simulations with a 25 grid square resolution have difficulty displaying the connected, round shape we expect from a herpetic lesion,

2.3. Simulations of HSV-2 Infection

these characteristics are displayed well at a 225 grid square resolution. This observation indicates that a high number of grid squares allows for a more accurate picture of lesion dynamics.

While the higher spatial resolution appears to produce a better representation of lesion development, further examination of these simulations, with X_1 and X_2 described as in equations 2.7 and 2.8, reveals a new issue. We see that lesions develop as an expanding ring, eventually surpassing the boundaries of the simulation region. This effect should not occur as the size of the simulation region was chosen to contain the largest of biologically realistic herpetic lesions. These dynamics can be explained by the nature of how the immune response has been defined. With virus dripping into the model region at the center grid site, infection most often begins here. As more epithelial cells become infected, CD8+ T cells are recruited to the site and begin attacking and clearing the infection from the center. However, virus is concurrently spreading to the surrounding grid sites. Since immune cell proliferation is only stimulated at sites where infected cells exist, immune presence at these sites is low when the virus first enters, allowing the virus to thrive. Immune cell response eventually catches up but, as the simulations show, can only chase, rather than prevent, infection spread. This phenomenon leads to the expanding ring we observe. To truly stop the infection, it would appear that increased immune cell presence needs to be stimulated in surrounding, uninfected sites to prevent the infection from spreading. This idea motivates a new definition for the terms X_1 and X_2 in the model and how immune cell production should be stimulated.

2.3. Simulations of HSV-2 Infection

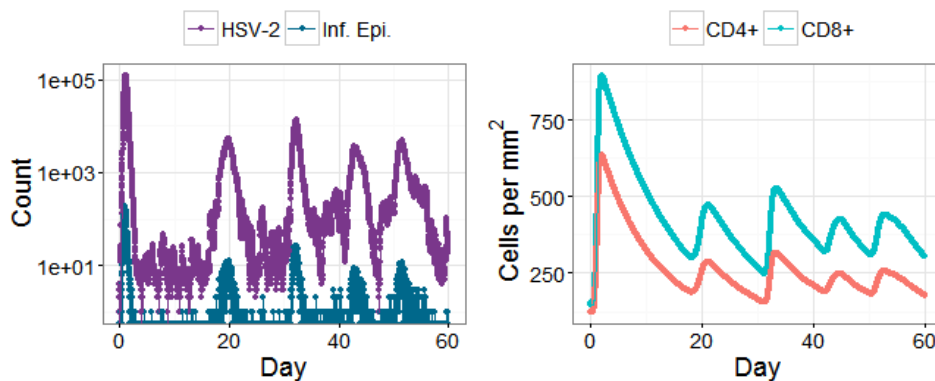


Figure 2.2: HSV-2 infection dynamics with no spatial resolution. Graphs depict counts of HSV-2 virus, infected epithelial cells, and CD4+ and CD8+ immune cells in the simulation region during one, sixty day, model run. Here, immune cell stimulation terms, X_1 and X_2 , are defined as in equations 2.7 and 2.8. All cells and virions within the system are assumed to be well mixed, with no spatial divisions. Infection dynamics show rapid infection development and extinction, with viral and immune cell loads corresponding with those found in the literature [34, 48]. Parameter values are the same as those reported in table 2.1, except $f = .003$ region/day, $\delta = 0.07$ /day, $\lambda = 2700$ /region-day, $\theta_1 = 2.84$ /day and $\theta_2 = 2.5$ /day.

2.3. Simulations of HSV-2 Infection

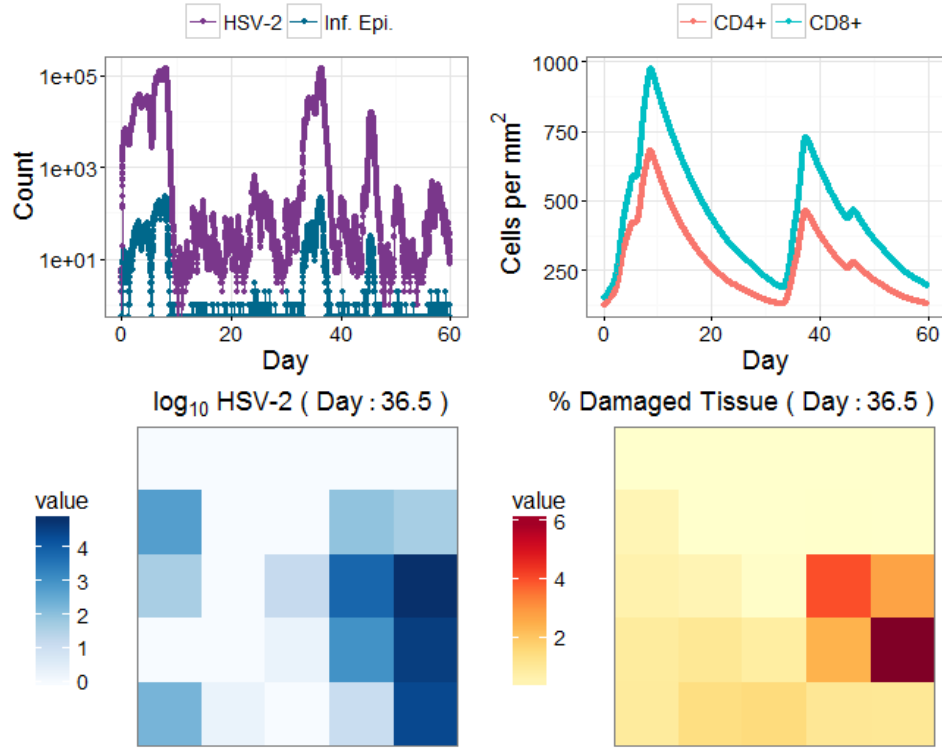


Figure 2.3: HSV-2 infection dynamics within a model region divided into a 5×5 grid. Immune cell stimulation terms, X_1 and X_2 , are defined as in equations 2.7 and 2.8. Upper graphs show the combined counts of HSV-2 virus, infected epithelial cells, and CD4+ and CD8+ immune cells in the entire simulation region during one model run. Lower graphs display spatially-specific counts of HSV-2 virus and the percent of tissue damage in each grid site taken at the time of the simulation’s highest viral load. While HSV-2 viral loads reach values over 10^4 virions in some grid sites, tissue damage due to the developing lesion remains low, ranging from 0-6% in each grid site.

2.3. Simulations of HSV-2 Infection

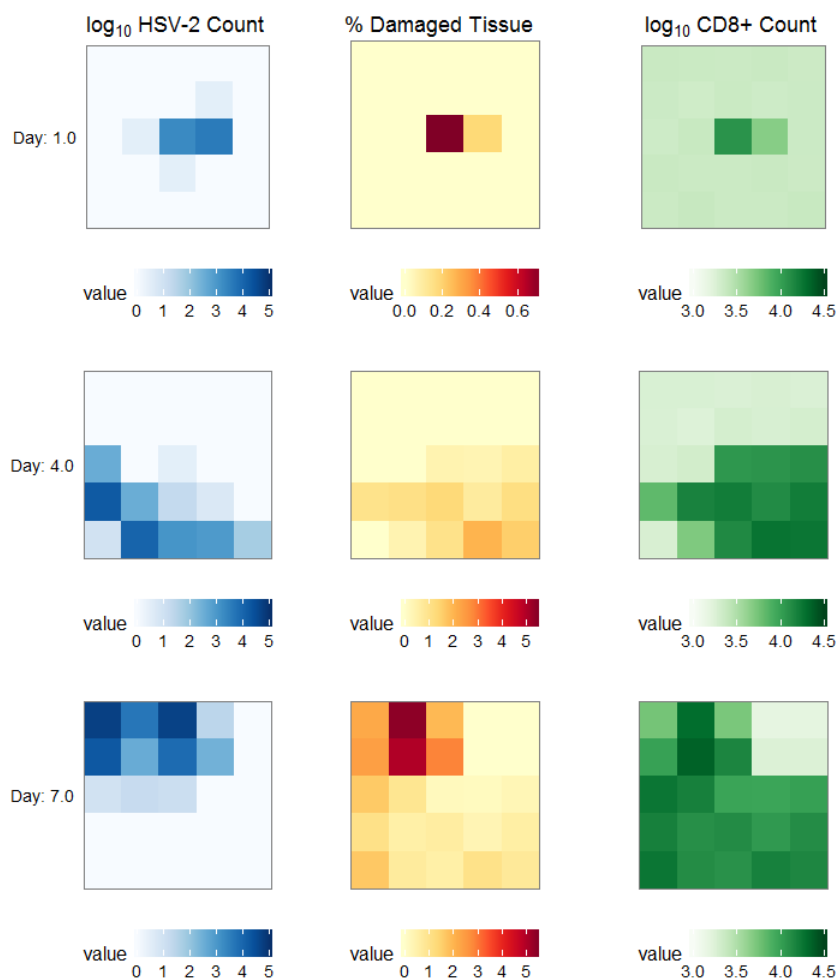


Figure 2.4: Stills taken from an HSV-2 infection simulation where the model region was divided into a 5×5 grid and X_1 and X_2 are defined as in equations 2.7 and 2.8. Stills show spatially resolved \log_{10} counts of HSV-2 virus (left), percent of damaged tissue (centre), and \log_{10} counts of CD8+ T cells (right) at days 1.0, 4.0 and 7.0 of the simulation. Note that scales change over panels. Infection begins at the center grid site, and spreads, leading to an increase in damaged tissue and the recruitment of CD8+ T cells. While capturing the spread of infection within the patch, the spatially resolved images present a poor representation of a rounded, connected lesion we expect in a herpes infection.

2.3. Simulations of HSV-2 Infection

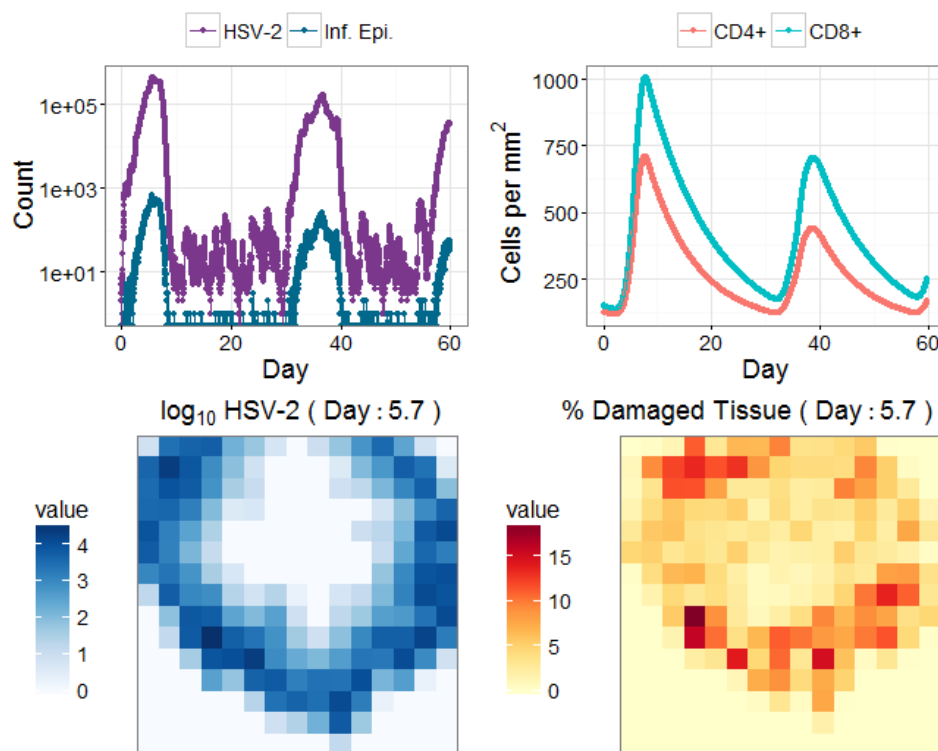


Figure 2.5: HSV-2 infection dynamics within a model region divided into a 15×15 grid. Immune cell stimulation terms, X_1 and X_2 , are defined as in equations 2.7 and 2.8. Upper graphs show the combined counts of HSV-2 virus, infected epithelial cells, and CD4+ and CD8+ immune cells in the entire simulation region during one model run. Lower graphs display spatially-specific counts of HSV-2 virus and the percent of tissue damage in each grid site taken at the time of the simulation's highest viral load. With the simulation being divided into a 15×15 grid, I obtain a clear visualization of a round, developing lesion; however due to the design of the model's immune response, infection develops as a spreading ring.

2.3. Simulations of HSV-2 Infection

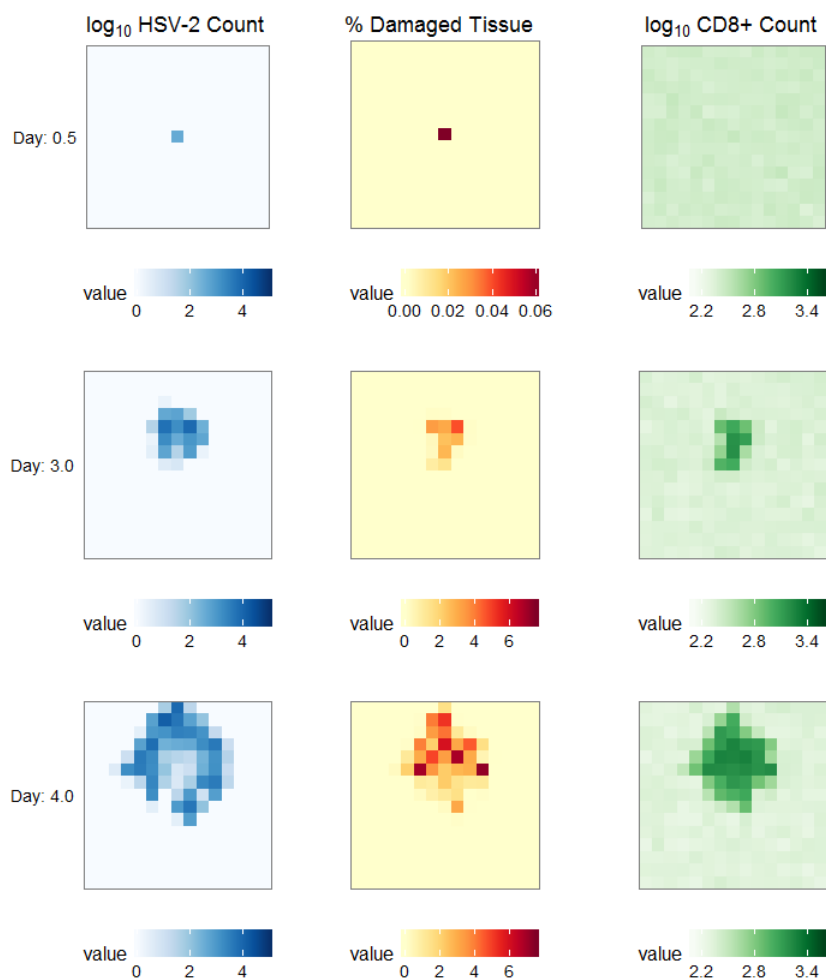


Figure 2.6: Stills taken from an HSV-2 infection simulation where the model region was divided into a 15×15 grid and X_1 and X_2 are defined as in equations 2.7 and 2.8. Stills show spatially resolved \log_{10} counts of HSV-2 virus (left), percent of damaged tissue (centre), and \log_{10} counts of CD8+ T cells (right) for the first seven days of the simulation. Note that scales change over panels. Infection begins at the center and grows quickly with viral counts reaching 10^4 and damaged tissue accounting for up to 30% of some grid sites. CD8+ T cells are recruited to the infection site; however, rather than being cleared, the infection develops into an expanding ring, eventually surpassing the boundaries of the simulation region.

2.3. Simulations of HSV-2 Infection

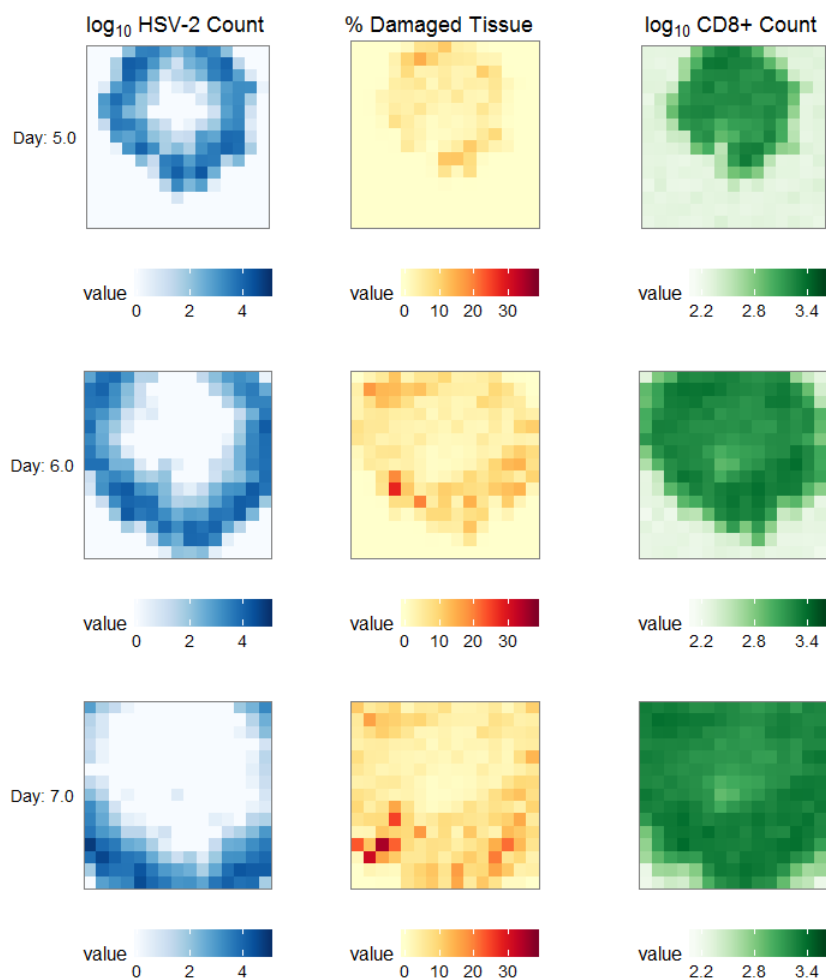


Figure 2.6 cont'd

2.3.2 Results of Model II for Immune Cell Proliferation

While capturing some of the dynamics seen in HSV-2 infections, executions of **Model I** failed to produce biologically accurate growth of a lesion. By implementing **Model II** as described in equations 2.9-2.12, I now account for the effects of cytokines on the system and their role in stimulating immune cell proliferation. Because cytokines are allowed to diffuse, immune cell proliferation can be stimulated away from the site of infection, potentially allowing immune cell response to get ahead of, and stop, the spreading ring of infection.

2.3. Simulations of HSV-2 Infection

To further the effects of cytokines on the model, I also took into account cytokines' ability to create a chemical gradient within tissue which existing immune cells migrate towards [28]. To capture this idea, I made the direction of immune cell diffusion dependent on the number of cytokines present in neighbouring grid squares. As the simulation ran, if at a given time step immune cell diffusion was the event chosen to occur, the program first checked the four neighbouring grid squares for cytokine presence. If none were present, then diffusion into any of the four neighbouring squares occurred with equal probability. However, if cytokines were present, the probability of diffusion into each of the neighbouring square was given by

$$Prob_{i,j} = \frac{C_{i,j}}{C_{tot}}, \quad (2.15)$$

with (i, j) taking on the indices of the four surrounding grid sites and C_{tot} being the total quantity of cytokines in these four sites. The full python code used to execute this model can be found in Appendix A.

Depictions of HSV-2 infection dynamics with the inclusion of cytokines are shown in figures 2.7-2.9. Again, the magnitude of viral and tissue damage peaks vary throughout a simulation, capturing the differences in lesion sizes and severities seen in patients. Stills of the simulation region throughout lesion development are shown in figure 2.8. In the absence of large lesions, runs often show small amounts of virus existing in the system, matching the asymptomatic viral shedding that is well described in chronically patients [34]. Occasionally, more severe infections become established in the tissue, leading to a greater viral peak and subsequently a high amount of tissue damage. The beginning of a viral peak appears to always correspond to times of low immune cell presence, suggesting a potential threshold in conditions needed for infection to break through. With the inclusion of cytokines in the model, virus and developing lesions are now cleared within the model region rather than surpassing its borders. These simulations present an excellent representation of the development of HSV-2 lesions in the genital tract, allowing me to move on and examine how the state of these developing lesions may dictate the probability of contracting HIV-1 upon exposure.

2.3. Simulations of HSV-2 Infection

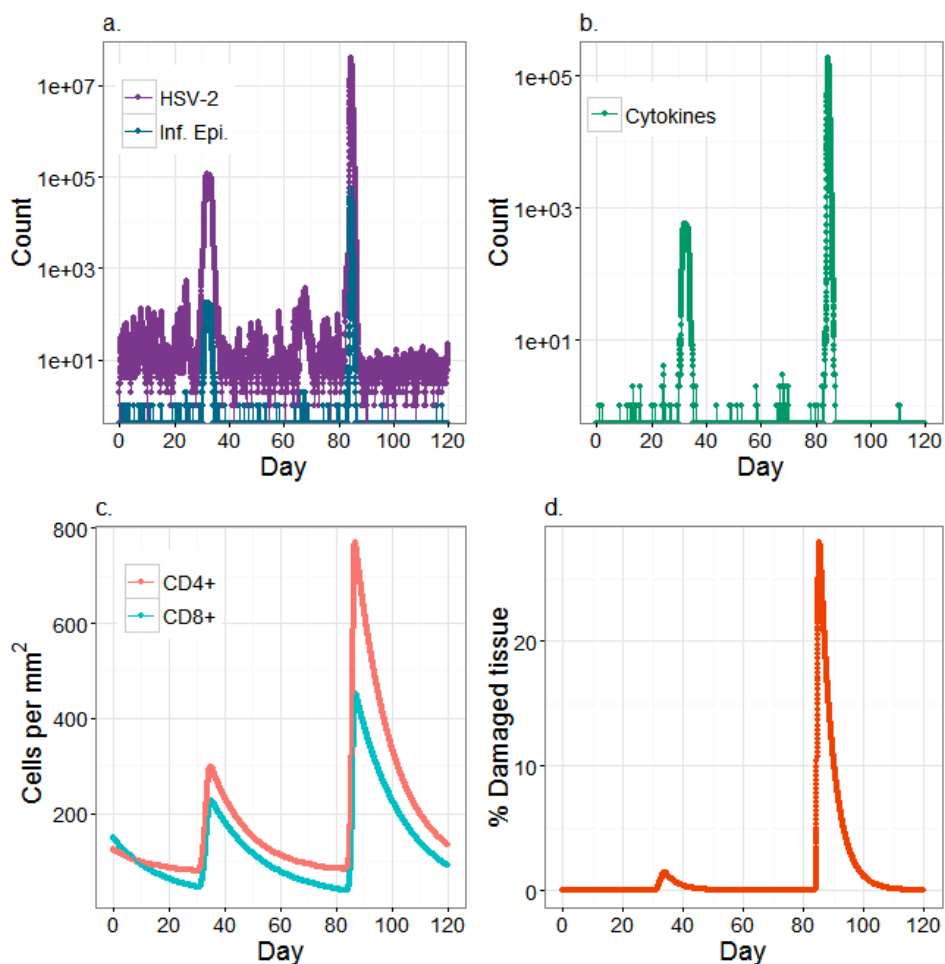


Figure 2.7: Summed HSV-2 infection dynamics for a single 120 day simulation within a model region divided into a 15×15 grid and with the inclusion of cytokines. Infection dynamics remain consistent with those in the literature [34, 48]. Graph a. shows how peaks in HSV-2 directly correspond with peaks in infected cells. Slightly delayed are the corresponding peaks of cytokines and immune cells shown in graphs b. and c. respectively. While the infection is cleared rapidly, tissue heals at a slower rate as depicted in graph d..

2.3. Simulations of HSV-2 Infection

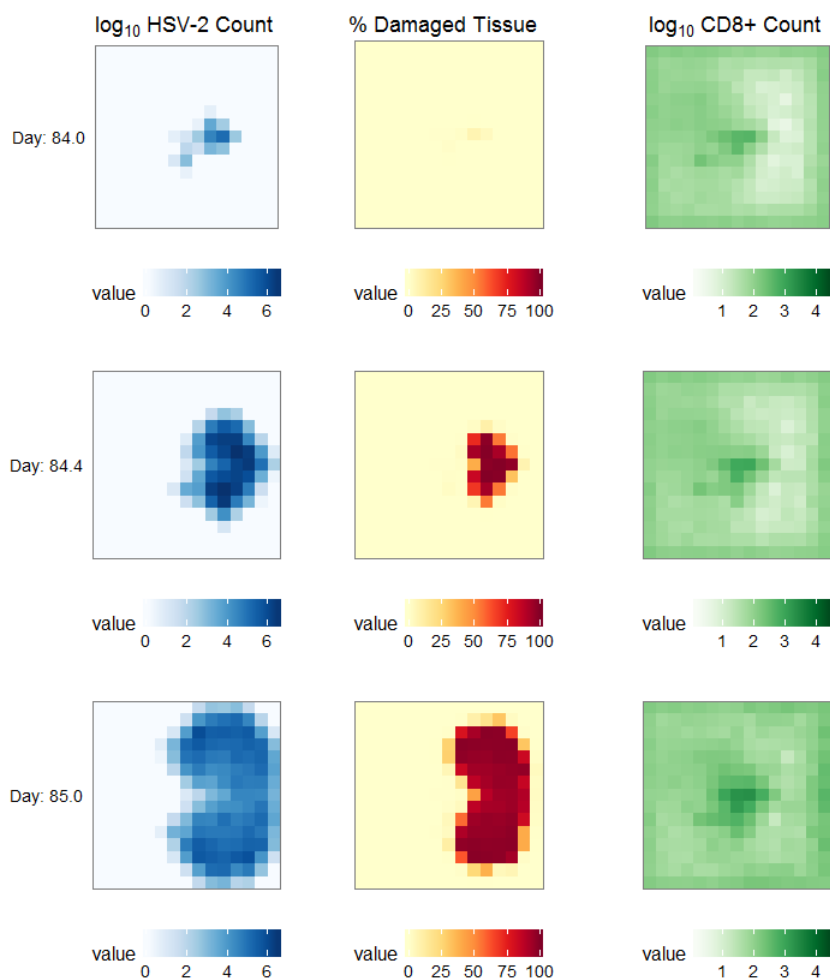


Figure 2.8: Stills of HSV-2 lesion development taken from a model simulation including the effects of cytokines. \log_{10} HSV-2 counts (left), percents of tissue damage due to lesion development (centre), and \log_{10} CD8+ immune cell counts (right) are shown across various days. Note that scales change across panels. With the inclusion of cytokines, simulations no longer present lesions developing as an expanding ring, but rather as a connected, growing patch. The lesion grows to a biologically realistic maximum size within the simulation area and then slowly heals. CD8+ immune cell presence becomes concentrated in areas of high infection, and remains at high, protective, concentrations even once virus has been cleared from the system.

2.3. Simulations of HSV-2 Infection

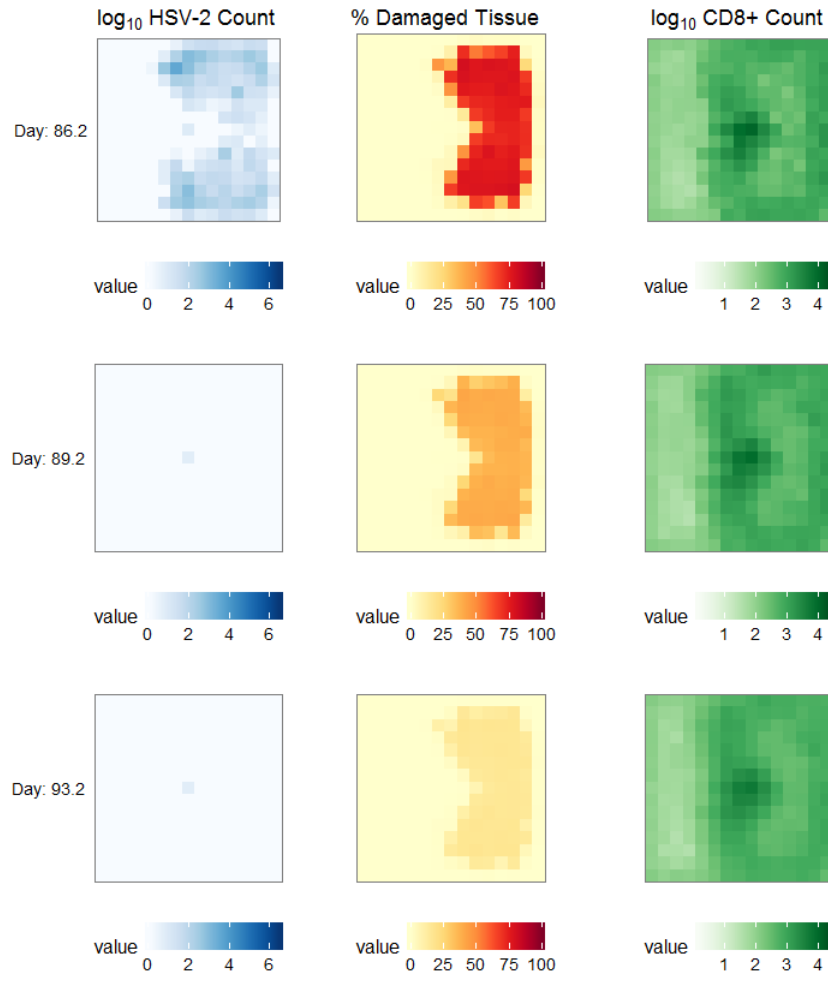


Figure 2.8 cont'd

2.3. Simulations of HSV-2 Infection

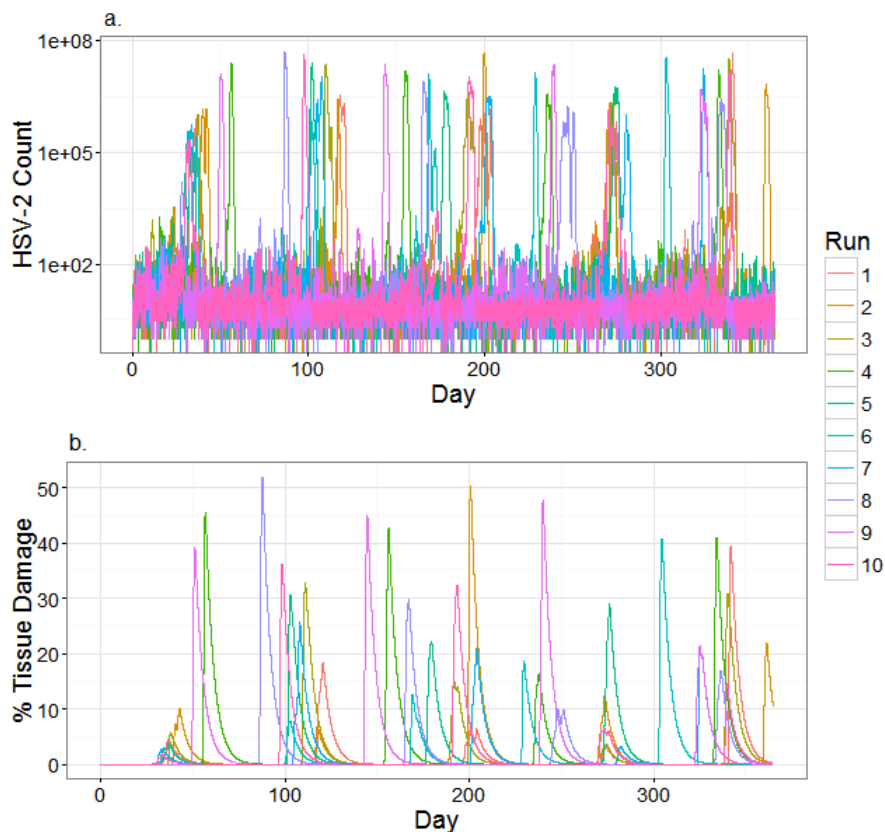


Figure 2.9: The results of ten simulations of chronic HSV-2 infection in a 4 cm^2 patch of the genital mucosa. The simulation region was divided into a 15×15 square grid and terms X_1 and X_2 of the model are defined as in equations 2.11 and 2.12. Graph a. shows the total quantity of HSV-2 over the whole simulation region and graph b. shows the total percent of tissue damage in the simulation region at all time points throughout year long simulations calculated using equation 2.14. Large variation exists between simulations, with each showing varying sizes of viral peaks and amount of tissue damage over time. At times of severe lesions, tissue damage can account for up to 50% of the 4 cm^2 patch of tissue, with HSV-2 counts reaching values close to 10^8 per simulation region.

Chapter 3

The Establishment of HSV-2 - HIV-1 Coinfection

3.1 A Description of HIV-1 Infection Dynamics

When HIV enters its host, it must infect a target cell in order for the infection to become established. These target cells are most commonly CD4+ T cells; however other immune cells expressing the CD4+ cell surface receptor such as tissue macrophages, and dendritic cells may also serve as a target. Once a cell is infected, it migrates to nearby draining lymph nodes where the virus gains access to a reservoir of immune cells. The virus replicates and infection propagates as infected cells spread throughout the blood stream. Previous experiments quantifying the immune presence in herpetic genital lesions show that the number of CD4+ cells greatly increases during lesional events [24, 48]. This result helps to explain why these patients show increased risks of HIV-1 contraction [14, 20]. By using the spatial stochastic model of the genital mucosa, I examined the initial establishment of HIV-1 infection in the tissue of patients with chronic HSV-2.

In order to examine how HIV-1 infection becomes established in an HSV-2 infected individual, I introduced HIV-1 virus into the modelled genital epithelial patch and tracked infection development. While the stochastic dynamics of the herpes infection remain as previously defined, I define new equations to describe the development of an HIV-1 infection as follows:

$$\Delta T_{i,j} = \left[\frac{\lambda}{n^2} + X_2 T_{i,j} - kn^2 T_{i,j} P_{i,j} - dT_{i,j} \right] \Delta t, \quad (3.1)$$

$$\Delta P_{i,j} = [\psi T_{2i,j} - kn^2 P_{i,j} T_{i,j} - \ell P_{i,j} + D_{P_{i,j}}] \Delta t, \quad (3.2)$$

$$\Delta T_{1i,j} = [kn^2 T_{i,j} P_{i,j} - \eta T_{1i,j} - g_1 T_{1i,j}] \Delta t, \quad (3.3)$$

$$\Delta T_{2i,j} = [\eta T_{1i,j} - g_2 T_{2i,j}] \Delta t. \quad (3.4)$$

CD4+ T cell dynamics now include loss due to infection by HIV-1 (P). This is set to occur through the properties of mass action at a rate propor-

3.1. A Description of HIV-1 Infection Dynamics

tional to kn^2 at each grid site, with n^2 being the number of grid squares in the simulation region. Once a CD4+ cell becomes infected, it moves into the T_1 class, representing latently infected cells known to be in the eclipse phase. These cells do not produce HIV-1 virus, but mature into actively infected cells (T_2) at a per-capita rate η . These actively infected CD4+ cells produce HIV-1 virus at a rate ψ and are cleared from the system at a rate g_2 . T_1 cells may be cleared from the system at a per-capita rate g_1 ; however, I assume that this rate is 0. The model includes no specific immune response against HIV-1-infected CD4+ cells as I assume no immunity against HIV-1 infection yet exists. These dynamics are again put into the spatial Gillespie framework with diffusion of HIV-1 occurring at a per-capita rate ω_P between neighbouring grid sites. The diffusion events for HIV-1 at grid site (i, j) are summarized by the term $D_{P_{i,j}}$ as described in equation 2.6 with $N = P$.

3.1.1 Defining HIV-1 Entry

HSV-2 infections are thought to increase HIV-1 infectivity in two ways: by providing an increased number of HIV-1 target cells, and causing tissue damage at the lesion site which serves as viral entry points. I therefore allow both of these factors to play a role in the probability of HIV-1 infection establishment.

The act of an HIV-1 virion penetrating the epithelium is a multi-step process. The virus must come in contact with the body, cross the genital mucus, and invade through the cells of the genital tract. The ability of virus to penetrate through the mucosa is variable and specific to the tissue exposed. The majority of human outer skin is composed of keratinized squamous epithelial cells which serve as a tough barrier for pathogenic invasion; however large portions of the genitals are composed of more delicate tissue. Regions that have direct contact with a partner's body fluid and are composed of a single layer or few layers of columnar epithelial cells, like the rectum, endocervix in women, and urethra in men, are the most susceptible to HIV-1 invasion [7, 19]. Areas consisting of squamous, non-keratinized, or poorly keratinized cells, like the inner foreskin in men, and ectocervix and vagina in women, are more protected, but still common other sites of HIV-1 invasion [7, 19]. HIV-1 transmission probabilities per sexual act range from 1 in 3000 to 1 in 20 depending on the genital tissue exposed, with the rectum being the site of highest risk [19, 30].

Recent *ex-vivo* experiments on initial HIV-1 infection in tissue samples taken from healthy females were used to estimate the number of HIV-1 virions able to penetrate the genital mucosa per sexual act [7]. When female

3.1. A Description of HIV-1 Infection Dynamics

genital tissue was exposed to a semen concentration of 5.0×10^3 HIV-1 virions/mL, characteristic of chronically infected semen loads in males not receiving standard antiretroviral therapy (ART), 18 virions were estimated to penetrate the epithelium of the vaginal surface per coital act [7]. Assuming the vaginal surface area is 88 cm^2 , this is approximately 0.2 virions/cm^2 [7]. When exposed to semen viral concentrations of 4.0×10^6 virions/mL, characteristic of acute HIV-1 infection in men not receiving ART, approximately 170 virions/cm^2 were predicted to pass through vaginal mucosa [7].

Using these values, I estimated the amount of HIV-1 virus that would pass through the epithelium and enter the model system per sexual act. To simulate a female with healthy genital epithelial tissue who engages in heterosexual intercourse with an HIV-1 positive partner not receiving ART, 1 virion per sexual act enters into the model region if the partner has a chronic HIV-1 infection, and 800 virions per sexual act enters the model region if the partner has an acute HIV-1 infection due to the 800 times higher viral load in the semen of acutely versus chronically infected men. I then modified these numbers based on the amount of lesional damage to the epithelium, allowing more virus to enter. In looking at the effects of weak cell junctions, Carias *et al.* 2013 found that 10 times as many viruses were able to penetrate the epithelium if weak cell junctions were present compared to tissue without weak cell junctions. Assuming the effects of lesion damage are similar, I used this estimate as a conservative representation of the increased amount of virus that enters due to damaged lesional tissue.

The amount of HIV-1 virus expected to enter the model region at grid site (i, j) in an individual exposed to chronic or acute HIV-1 viral loads respectively is described as follows:

$$P_{\text{chronic},i,j} = \frac{1 + 9L_{i,j}}{n^2}, \quad (3.5)$$

$$P_{\text{acute},i,j} = \frac{800 + 7200L_{i,j}}{n^2} = 800P_{\text{chronic},i,j}. \quad (3.6)$$

$L_{i,j}$ measures tissue damage as defined in equation (2.9). Summing over all grid sites, we can obtain the total amount of virus expected to enter the system:

$$P_{\text{chronic,tot}} = \sum_{\forall i} \sum_{\forall j} P_{\text{chronic},i,j}, \quad (3.7)$$

$$P_{\text{acute,tot}} = \sum_{\forall i} \sum_{\forall j} P_{\text{acute},i,j}. \quad (3.8)$$

3.1. A Description of HIV-1 Infection Dynamics

If no lesion is present in the model region ($L_{i,j} = 0 \forall(i, j)$), then the previously mentioned estimates of 1 or 800 HIV-1 viruses per simulation region are allowed to enter. These values increase linearly with tissue damage leading to 10 times more virus entering the tissue if it is entirely damaged ($L_{i,j} = 1 \forall(i, j)$).

3.1.2 Parameters for HIV-1

Many mathematical models have examined initial HIV-1 infection, leading to a rich supply of previously determined parameter values. However, few explicitly examined the dynamics occurring within the epithelium, the most common site of HIV-1 infection establishment. As HIV-1 and immune cell counts usually come from blood or plasma samples, the parameters of most models are fit to these numbers [10, 31, 39]. While dynamics occurring within the blood and epithelium may be similar, they may not be occurring at the same rates. While I was able to choose some parameter values based on those used in previous models, others were estimated based on our knowledge of HSV-2 infection behaviour in the genital mucosa. This is with specific reference to the estimates for parameters ψ and ℓ . As only within-blood estimates have been recorded in the literature for these parameters, I chose values that corresponded with those fit for HSV-2 dynamics. Here, ψ matches with the rate of HSV-2 production and ℓ matches with the value for HSV-2 clearance. All HIV-1 parameters used in the model are listed in table 3.1.

Table 3.1: List of parameter values used in the model to describe HIV-1 infection dynamics

	Units	Value Chosen	Range in Literature	Citation
k	region/day	1×10^{-7}	3.7×10^{-8} – 7.4×10^{-4}	[10, 29]
ψ	/day	7.05×10^3	2×10^4	[10]
ℓ	/day	8.8	20 – 23	[10, 29]
ω_P	cm ² /day	7.2×10^{-4}	2.8×10^{-6} – 3.1×10^{-3}	[5, 25, 27]
η	/day	1	0.7 – 5	[10, 29]
g_1	/day	0	0 – 0.5	[10, 29]
g_2	/day	1.2	0.583 – 1	[10, 29]

3.1.3 The Dynamics of HIV-1 Infection

To represent exposure to the HIV-1 virus, I paused the simulation at various states of lesion development, introduced the calculated amount of HIV-1

3.1. A Description of HIV-1 Infection Dynamics

virus depending on the current lesion state, and then restarted the simulation. An example run showing HIV-1 infection establishment upon exposure to an acute load of HIV-1 is shown in figure 3.1. In this scenario, HIV-1 virus was introduced during a peak lesion event. From this figure we can see that the infection establishes quickly, with HIV-1 viral loads approaching 10^6 in the tissue within four days of infection. Figure 3.2 shows the spatial dynamics occurring during this infection. Virus is introduced, and while most virus quickly dies off, infection becomes prominently established at one site and quickly develops there. We can note that after less than four days of HIV-1 infection, the number of target CD4+ cells at the infection site have been depleted. While this may imply that target cell abundance may limit HIV-1 infection expansion, it is important to keep in mind that this model does not include the migration of infected cells to the lymph nodes where the virus can find another large reservoir of target cells. However, we clearly note the fast establishment and importance of target cell number in the epithelium during HIV-1 infection.

3.1. A Description of HIV-1 Infection Dynamics

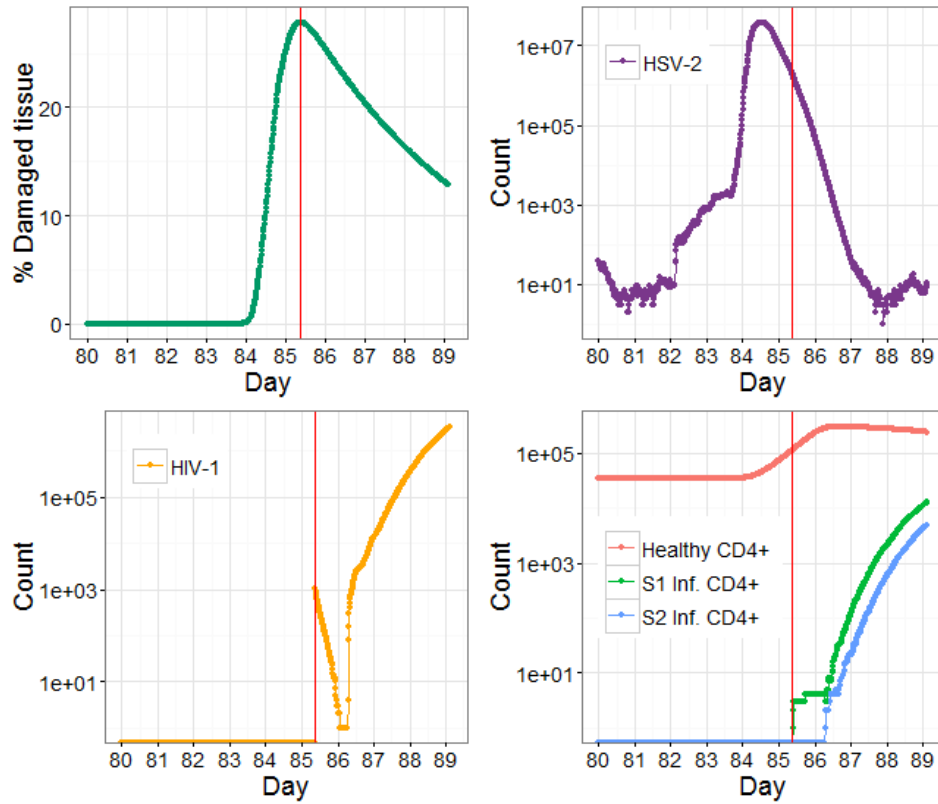


Figure 3.1: Dynamics of HIV-1 infection establishment in an HSV-2 positive patient upon exposure to an acute dose of HIV-1 in the semen. Here, the vertical red line indicates the time of HIV-1 introduction into the simulation region. Plots show the amount of tissue damage due to HSV-2 lesions, the amount of HSV-2, and the number of healthy CD4+ T cells before and after HIV-1 introduction. Also shown are the changing HIV-1 counts, number of infected CD4+ cells in the eclipse phase, and number of infected CD4+ cells in the active phase once HIV-1 has been introduced. By day 89 of the simulation, 4 days after the HIV-1 transmission event, HIV-1 counts and the number of infected CD4+ cells are high enough for the HIV-1 infection to be considered fully established with little chance of it being cleared from the system.

3.1. A Description of HIV-1 Infection Dynamics

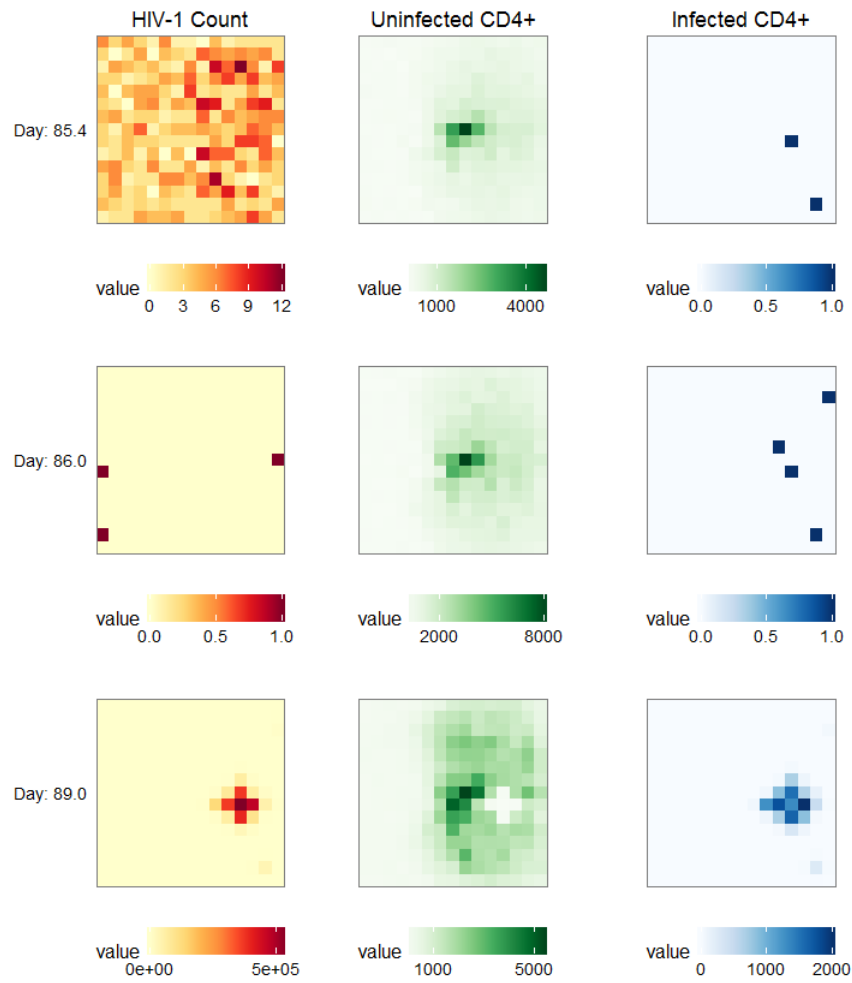


Figure 3.2: Spatial dynamics of HIV-1 introduction for the same simulation region as shown in Figure 3.1. HIV-1 counts (left), uninfected CD4+ T cell counts (centre), and infected CD4+ T cell counts (left) are shown across the initial days of infection. Note that scales change across panels. HIV-1 enters on day 85.4 of an HSV-2 infection simulation and quickly becomes established.

3.2 Determining HIV-1 Infection Probability

While individual runs of the model give information on how the HIV-1 infection first becomes initialized, many repetitions of these simulations need to be performed in order to approximate the probability of HIV-1 infection establishment. One issue with this approach is the great amount of time required to complete each full simulation. Tracking both the HSV-2 and HIV-1 dynamics is computationally expensive and therefore performing many simulations that record all the dynamics is unrealistic. To minimize computational time but still gather the data necessary to calculate HIV-1 infection probability, I tracked only the dynamics related to HIV-1 infection establishment once HIV-1 virus was introduced into the simulation region. By making this simplification, I assume that the changes in HSV-2 infection dynamics have a minimal effect on CD4+ T cell count during the small time window during which HIV-1 infection establishment occurs.

To calculate the probability of HIV-1 infection in patients with different HSV-2 lesion scenarios, I used the following algorithm:

1. Stop an HSV-2 infection simulation at a point where exposure to HIV-1 is assumed to occur.
2. Calculate the fraction of tissue damage at each simulation grid site using equation 2.13.
3. Calculate the total number of HIV-1 viruses expected to enter the simulation region using equation 3.7 or 3.8, depending on the type of exposure being examined, and round it to the closest whole virus.
4. Randomly distribute these viruses among the grid sites of the simulation region following a multinomial distribution with the probability of a virus being distributed to site (i, j) given by

$$\text{Prob}_{\text{chronic},i,j} = \frac{P_{\text{chronic},i,j}}{P_{\text{chronic,tot}}} \quad (3.9)$$

or

$$\text{Prob}_{\text{acute},i,j} = \frac{P_{\text{acute},i,j}}{P_{\text{acute,tot}}}. \quad (3.10)$$

depending on the situation being simulated.

5. Isolate and simplify the dynamics occurring within each grid site to only include the main components involved in HIV-1 infection (dynamics of T , T_1 , T_2 , P and C).

3.2. Determining HIV-1 Infection Probability

6. For each grid square, run the Gillespie algorithm for the simplified dynamics, stopping the simulation once the infection has gone extinct or propagated enough to imply infection establishment. Here, I assume that infection is established once the simulation region has at least 8 infected cells [31].
7. Repeat steps 4. to 6. 10,000 times.
8. For every grid square (i, j) , define the probability of HIV-1 infection at that site, $\text{Prob}_{\text{inf},i,j}$, as the fraction of successful infections that occurred at that site over the 10,000 simulations.
9. Combine the probabilities of infection at each grid site to achieve an overall probability of HIV-1 infection for the entire simulation region. To do this, I look at the probability that infection becomes established in any of the grid squares of the simulation region using the formula

$$\text{Prob}_{\text{inf,tot}} = 1 - \prod_{\forall i} \prod_{\forall j} (1 - \text{Prob}_{\text{inf},i,j}) \quad (3.11)$$

where $\text{Prob}_{\text{inf,tot}}$ is the overall probability of HIV-1 infection over the entire simulation region.

Examples of the results obtained from these simulations appear in figures 3.3 and 3.4. In total, I examined 26 different simulated tissue samples experiencing various states of lesional damage. In particular, I focused on HIV-1 exposure to tissue that was healthy with no HSV-2 infection, tissue exposed one week before peak tissue damage, tissue exposed during peak tissue damage, tissue exposed during peak CD4+ T cell levels, and tissue exposed one, two, or four weeks after peak tissue damage. These initial conditions are summarized in table 3.2. Each tissue sample was exposed to HIV-1 counts representative of the amount within the semen of chronically and acutely infected males, leading to a total of 52 infection simulations.

3.2. Determining HIV-1 Infection Probability

Table 3.2: Simulation scenarios used to find HIV-1 infection probabilities. Simulations were paused at different times of lesion development, creating a sample scenario of when tissue may become exposed to HIV-1.

Simulation Initial Conditions	# of Samples	Ave CD4+ cell count/mm ² Across Samples	Ave % Tissue Damage Across Samples
healthy	1	40.00	0
1 week before peak lesion	4	83.75	0.000850
peak lesion	5	448.6	18.3
peak CD4+ cell count	2	872.5	15.5
1 week after peak lesion	5	605.0	4.52
2 weeks after peak lesion	5	392.8	0.983
4 weeks after peak lesion	4	200.0	0.113

Since the model assumes chronic HSV-2 infection, I had to make modifications in order to simulate healthy tissue. The simulations representing HIV-1 infection in healthy tissue were started with 16000 CD4+ T cells randomly distributed throughout the simulation region, corresponding with the equilibrium concentration of CD4+ T cells in healthy epidermis as recorded in the literature [48]. All HSV-2 virus, HSV-2 specific CD8+ T cell, and HSV-2 infected cell dynamics were also removed. Since this system is comparatively resistant to infection due to having no tissue damage and low CD4+ T cell numbers, the above algorithm was modified slightly with the simulation being repeated 50,000 times rather than 10,000 times so that the low probability of infection in healthy tissue could be captured.

3.2. Determining HIV-1 Infection Probability

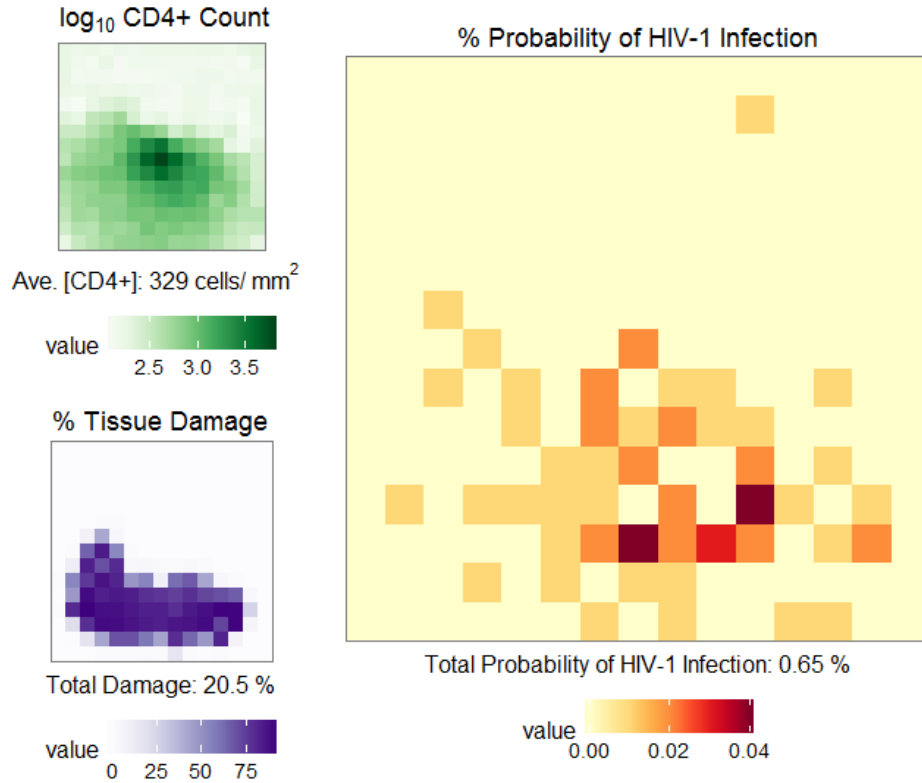


Figure 3.3: Per-coital act probability of HIV-1 infection in one simulation region upon exposure to HIV-1 from a chronically infected partner. Here, HIV-1 was entered into the simulation region during the peak of an HSV-2 lesion. CD4+ T cell counts per mm² and the amount of tissue damage in the simulation region at the time of exposure are shown on the left. The figure on the right depicts the probability of an HIV-1 infection becoming established at each grid site. Combining these probabilities, as described in equation 3.11, leads to a 0.65% risk of HIV-1 infection establishment somewhere within this model region.

3.2. Determining HIV-1 Infection Probability

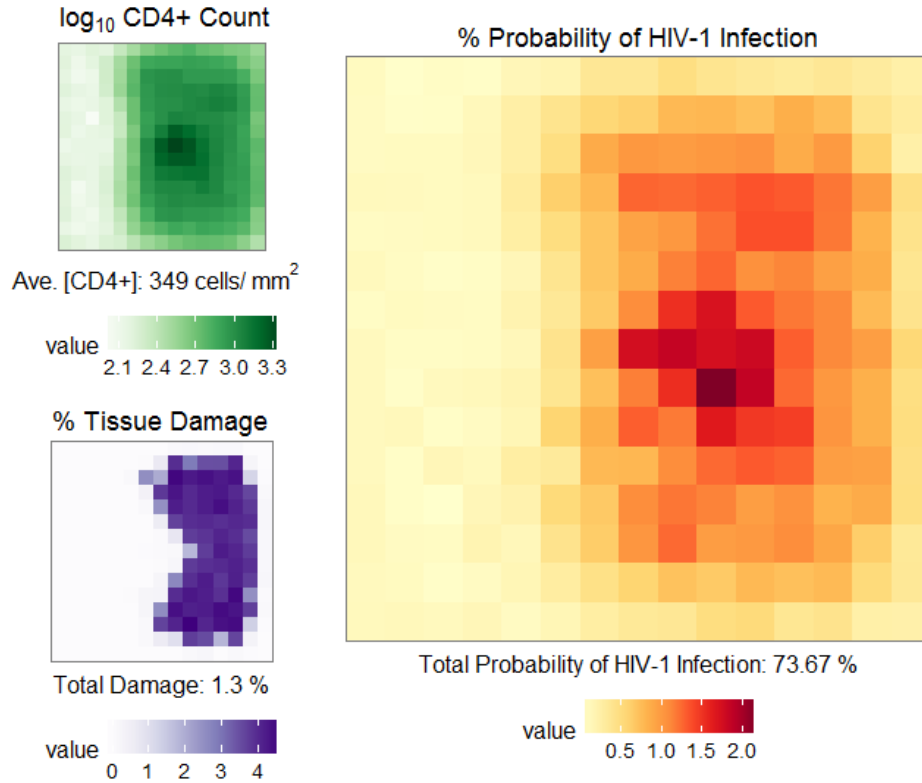


Figure 3.4: Per-coital act probability of HIV-1 infection in one simulation region upon exposure to HIV-1 from an acutely infected partner. Here, HIV-1 was entered into the simulation region two weeks after the peak of an HSV-2 lesion. CD4+ T cell counts per mm² and the amount of tissue damage in the simulation region at the time of exposure are shown on the left. The figure on the right depicts the probability of an HIV-1 infection becoming established at each grid site. Combining these probabilities, as described in equation 3.11, leads to a 73.67% risk of HIV-1 infection establishment somewhere within this model region. This risk seems unrealistically high indicating an issue with our description of HIV-1 entry and infection development in the acute scenario.

The probability of HIV-1 infection for each of the 52 infection simulations, plotted against the number of CD4+ T cells and amount of tissue damage at the time of HIV-1 introduction, appears in figure 3.5. By fitting linear planes to the data, the probability of HIV-1 infection can be expressed as a function of CD4+ T cell number and tissue damage. The

3.2. *Determining HIV-1 Infection Probability*

linear planes were forced to pass through the points representing HIV-1 infection probability in healthy tissue in each scenario in order to fully capture the background risks of infection. These equations appear at the top of the graphs in figure 3.5.

3.2. Determining HIV-1 Infection Probability

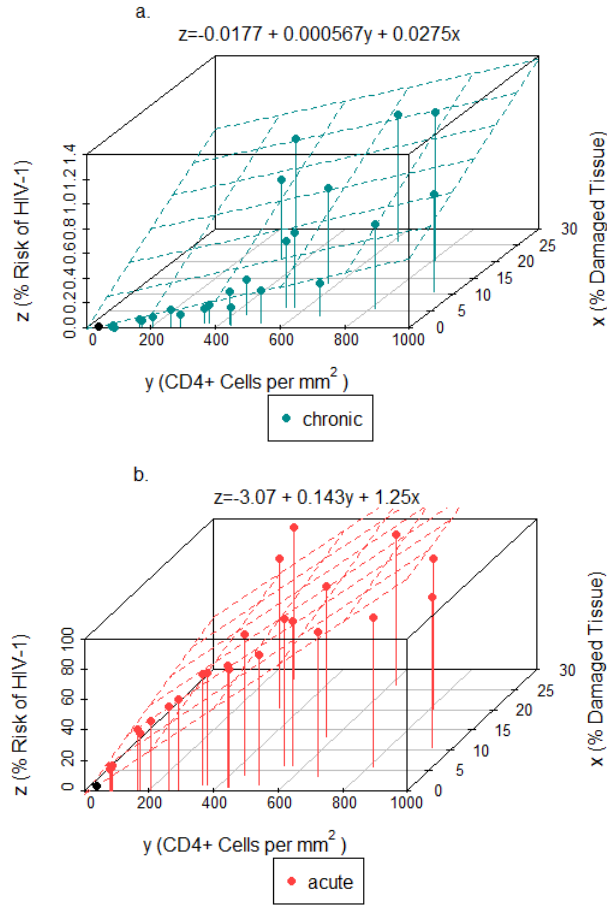


Figure 3.5: Probability of HIV-1 infection in a $2\text{ cm} \times 2\text{ cm}$ region exposed to an acute or chronic dose of HIV-1 in semen. Graphs a. and b. show data collected during chronic and acute HIV-1 exposure simulations respectively. Here, risk of HIV-1 is plotted against the number of CD4+ T cells per mm^2 and the percent of herpetic lesional tissue damage taking up the simulation region at the time of HIV-1 introduction. Through linear regression, I found planes of best fit, describing HIV-1 infection risk as a function of tissue damage and CD4+ T cell count. Planes of best fit were made to pass through the points describing HIV-1 infection in healthy tissue, shown in black, in order to capture the background risk of infection. Equations from the linear regression of the simulated data appear above their respective graphs and show good fit with the R^2 values being 0.9703 and 0.9204 for graph a. and b. respectively.

3.2. Determining HIV-1 Infection Probability

While the infection probabilities predicted by the model for chronic HIV-1 exposure seem plausible, those predicted for acute HIV-1 exposure seem unrealistically high. In healthy tissue, the probability of HIV-1 infection per simulation site was 0.005% per sexual act when exposed to chronic HIV-1 viral loads and 2.7%, a 540 fold increase, per sexual act when exposed to acute HIV-1 viral loads. Similar comparisons of acute and chronic HIV-1 risks appear in table 3.3. HIV-1 infection probability is known to increase when individuals are exposed to acute rather than chronic HIV-1 viral loads, however studies have reported this to only be a 4.3 fold increase [32]. While this value is with respect to infection anywhere within the genital region and the simulations here only report values with respect to infection risk in one 4 cm² patch of genital epithelium, the increase seen from the results of the model appears to be too high.

Table 3.3: Fold increases in per-coital HIV-1 risk when comparing exposure to chronic versus acute HIV-1 viral loads. For all tissue samples used to simulate HIV-1 infection probabilities, risks of HIV-1 were significantly higher when tissue was exposed to acute doses of HIV-1 opposed to chronic doses of HIV-1.

Simulation Initial Conditions	Ave Risk of HIV-1 (chronic exposure)	Ave Risk of HIV-1 (acute exposure)	Fold Increase
healthy	0.005%	2.7%	540
peak tissue damage/ peak CD4+ cell number	0.79%	98.94%	125
mild to moderate tissue damage	0.19%	59.97%	316

There are a few reasons as to why the model may have predicted unrealistically high infection probabilities in patients exposed to acute HIV-1 viral loads. The first may be due to how I define infection establishment. In the model, the infection is considered established once the HIV-1 infection has managed to infect eight CD4+ cells. Even at this point there is a small possibility that the infection could be cleared. Other models have had thresholds of 32 infected CD4+ cells [31]. Having a higher threshold would likely decrease the frequency of HIV-1 infection; however how this would affect the relative increase in infection risk between chronic versus acute HIV-1 viral load exposures remains unclear. Another explanation may be rooted in the number of infectious HIV-1 virions assumed to be in acute HIV-1 seminal loads. While I assume that all viruses that enter the system are equally infectious and qualitatively the same in both chronic and acute

3.2. Determining HIV-1 Infection Probability

semen loads, this may not be the case. If the HIV-1 virions produced during the acute phase of infection could be shown to be less infectious than the virions produced later in infection, this could help explain why the results here on infection probabilities from exposure to acute HIV-1 viral loads are too high. Further, I may have overestimated the number of HIV-1 virions able to penetrate the epithelium. While my calculations are based on the estimate that 170 virions/cm² are able to penetrate the healthy genital mucosa when exposure to acute loads of HIV-1 occurs [7], this estimate does not consider how mucus on the surface of the tissue may hinder viral entry. Serving as a barrier to the epithelium, mucus is thought to protect against infection and may reduce the number of HIV-1 virions an individual is exposed to and decrease infection risk. Finally, the clearance rate of HIV-1 was chosen to match with the clearance rate of HSV-2 in the genital epithelium since no within-epithelium estimates for this parameter are currently available in the literature. This parameter choice is approximately three times smaller than those estimates for this parameter in the blood [10, 29]. Allowing for a rate of HIV-1 clearance similar to that seen in the blood would likely decrease the risk of HIV-1 acquisition; however it is difficult to know which parameter value is best given the limitation of data on HIV-1 dynamics in the genital epithelium. This point stresses the importance of further study of HIV-1 initial infection in the epithelium.

While the HIV-1 infection risks for exposure to acute HIV-1 viral loads appear unrealistically high, those for exposure to chronic HIV-1 can help inform both clinicians and HSV-2 infected individuals of the per-coital risks of HIV-1 contraction and when to take the most caution in sexual activities with HIV-1 positive partners. I next use the relationships between HSV-2 infection state and HIV-1 risk to determine how doses of HSV-2 antivirals may reduce these infection probabilities. I however continue my analysis solely for HIV-1 infection upon exposure to chronic HIV-1 viral loads.

Chapter 4

Effects of HSV-2 Antivirals on HIV-1 Infection Probability

While there is currently no vaccine or cure for HSV-2 infection, many HSV-2 patients receive antiviral treatment to help control their lesion outbreaks. The most commonly prescribed drug is acyclovir and variants thereof. These drugs work by inhibiting the virus's DNA polymerase, preventing replication [1]. While not suppressing the HSV-2 virus entirely, acyclovir and its variants decrease HSV-2 shedding and lesion development. Theoretically, with a decrease in the amount of virus and number of lesions, patients should experience a decreased risk of contracting HIV-1; however, clinical studies have had difficulty detecting this effect [8, 18, 46]. Studies have shown equal probability of HIV-1 contraction for HSV-2 positive patients independent of whether they are receiving acyclovir [8, 18, 46]. Here, I work to understand why this anomaly occurs and form a mathematical prediction of HSV-2 antiviral drug doses needed to significantly decrease an individual's risk of acquiring HIV-1.

4.1 Impact of Antivirals on HSV-2 Infection and Lesion Development

To account for the effects of HSV-2 antiviral drugs in the mathematical model designed to describe chronic HSV-2 infection in the genital mucosa, I include a new parameter ζ to describe the effectiveness of anti-virals in suppressing HSV-2 replication. Here, ζ can take values in $[0, 1]$ with 0 representing an antiviral dosage that has no effect on HSV-2 replication and 1 representing complete suppression of replication. I assume this suppression decreases both the amount of virus that drips out of the neurons and the amount of virus an infected epithelial cell produces. The modified HSV-2 viral dynamics are described as follows:

4.1. Impact of Antivirals on HSV-2 Infection and Lesion Development

$$\Delta V_{i,j} = [\phi(1 - \zeta) + p(1 - \zeta)I_{i,j} - \beta n^2 H_{i,j} V_{i,j} - cV_{i,j} + D_{V_{i,j}}] \delta t. \quad (4.1)$$

I analyzed four potential values for ζ ($\zeta = 0.15$, $\zeta = 0.5$, $\zeta = 0.7$, $\zeta = 0.85$) and studied the resulting effects on lesion dynamics.

One of the most recent antivirals for HSV-2 treatment, currently in clinical trial, is pritelivir. It reduces HSV viral loads by targeting the DNA helicase of HSV and is considered a stronger drug option for HSV treatment [37]. Development of these new drugs is important as some resistance to previous HSV-2 antivirals has been observed [22]. Recent clinical trial data have been released on the effectiveness of pritelivir at different doses [44]. Previous analysis of this data predicts the following relationship between viral shedding reduction, an empirical equivalent to ζ , and daily pritelivir dose [37]:

$$\% \text{ reduction} = 30.1 \ln(\text{daily dose}) - 51.5, \quad (4.2)$$

with daily dose being measured in milligrams. From this function, we can inversely infer that

$$\text{daily dose} = e^{\frac{\zeta + 0.515}{0.301}}. \quad (4.3)$$

Using this formula and rounding the daily dose to the closest 5 milligrams, the ζ values being used correspond to doses of 10, 30, 55, and 80 mg a day. These amounts all fall within the range of pritelivir doses given to patients in recent drug trials [44]. While other models have included the pharmacokinetics and pharmacodynamics of the drug in the body [37], I assume the patient has a constant dosage within their body for simplicity. This assumption can be considered acceptable due to pritelivir's long 80-hour half-life which keeps drug conditions within the body relatively constant [37].

Using the new definition for the dynamics of the HSV-2 virus that includes antiviral effects, I ran the stochastic Gillespie algorithm as described previously and examined the characteristics of the lesions that developed under these four drug scenarios. Specifically, I compared fifty, one-year simulations of the model for each of the four treated cases and the untreated case, counting the number of viral peaks and lesions that occurred in each run, and the duration of each lesion episode. I classified a viral peak as a spike of virus greater than 1000 virions with no higher viral counts within the five previous and following days. Similarly, lesion peaks were classified

4.1. Impact of Antivirals on HSV-2 Infection and Lesion Development

as tissue damage taking up at least 1% of the simulation region and with no higher levels of tissue damage within the five previous and following days. To measure the duration of a lesion, the lesion was assumed to begin when tissue damage was greater than 1% of the simulation region and was considered over when tissue damage dropped below 1% of the simulation region. If a lesion episode was to occur within five days of a previous one, it was classified as the same lesion event. These results are summarized in figures 4.1-4.3. Results show that as pritelivir dose increases, the severity of viral and lesion peaks, and the duration of lesions, decrease. The frequency at which viral peaks and lesions occur also decrease with higher pritelivir doses. When compared to simulations of HSV-2 positive patients receiving no treatment, lesions are two times less frequent and last half as long due to their decreased severity.

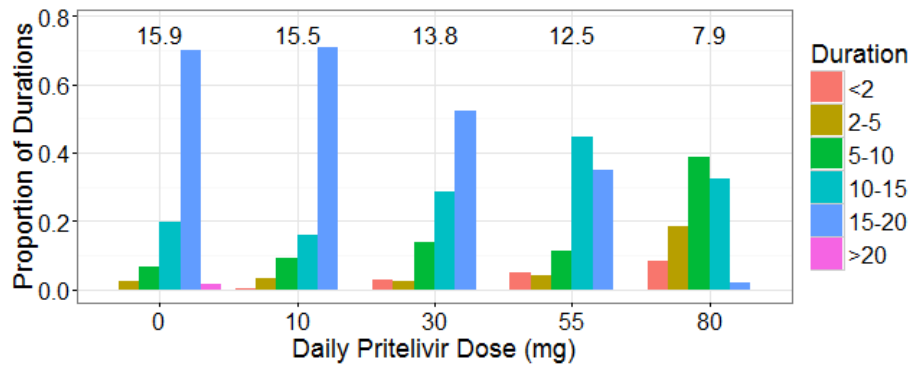


Figure 4.1: Pritelivir’s effect on lesion duration during HSV-2 infection. Here, the duration of HSV-2 lesions at varying doses of pritelivir was calculated and categorized based on length. A lesion was defined to begin when tissue damage due to HSV-2 infection was greater than 1% of the simulation region and considered healed once tissue damage dropped below 1%. The duration of all lesions is reported in days. Numbers appearing at the top of the graph represent the average number of days lesions lasted for simulations run at each dose of pritelivir. Lesion duration decreases as pritelivir dose increases due to smaller lesions that occur.

4.1. Impact of Antivirals on HSV-2 Infection and Lesion Development

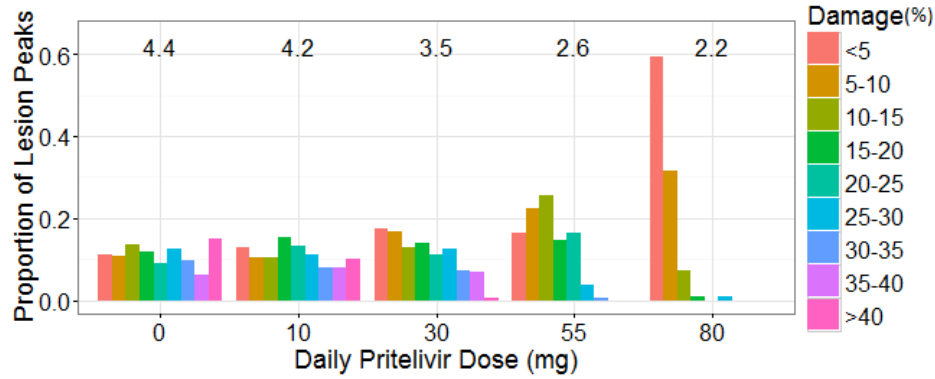


Figure 4.2: Pritelivir’s effect on tissue damage during HSV-2 infection. Here, the percent of tissue damage at times of peak lesions for varying doses of pritelivir was calculated and categorized based on its severity. Peak lesions were defined as when the greatest fraction of epithelial cells were absent from the system due to infection-caused cell death. Numbers appearing at the top of the graph represent the average number of lesions that occur in a one-year simulation for each dose of pritelivir. The frequency and severity of HSV-2 lesions decrease as pritelivir dose increases.

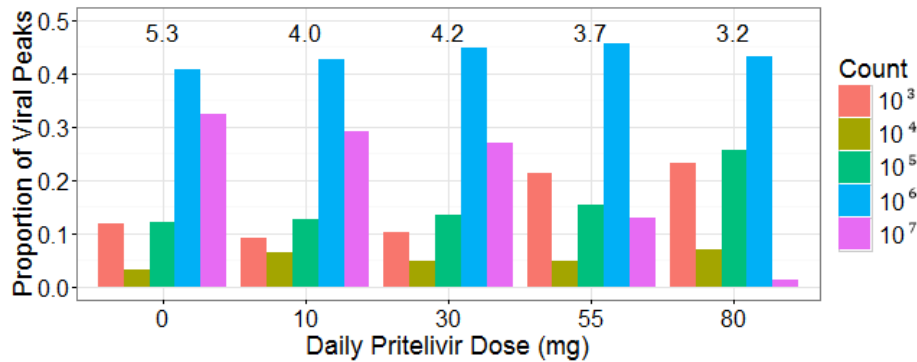


Figure 4.3: Pritelivir’s effect on viral shedding during HSV-2 infection. Viral peaks that occurred during model simulations run at varying doses of pritelivir were counted and classified based on their magnitude. Numbers appearing at the top of the graph represent the average number of viral peaks occurring in a one-year simulation for each dose of pritelivir. While viral peaks are slightly worse at a dose of 10 mg/day compared to 30 mg/day, the general trend shows that as pritelivir dose increases, both the frequency and severity of HSV-2 viral peaks decrease.

4.2 Pritelivir's Impact on HIV-1 Infection Probability

With an understanding and mathematical representation of how antiviral HSV-2 drugs decrease the severity of herpes lesions and infections, it would be valuable to determine if and by how much this drug may decrease the probability of contracting HIV-1 in patients who are HSV-2 positive and facing HIV-1 exposure.

As presented in Chapter 3, HIV-1 infection probability per simulation site can be estimated by the equation

$$Prob_{inf,tot} \approx -0.0177 + 0.000567T + 0.0275L \quad (4.4)$$

for each sexual act with a chronically infected individual. Here T represents the per mm^2 average number of CD4+ T cells and L represents the total percent of tissue damage in the simulation region upon the time of exposure to HIV-1. By observing how CD4+ T cell counts and lesion damage change in patients being treated with HSV-2 antivirals, I obtained a representation of how these drugs may decrease the probability of infection.

Median HSV-2, CD4+ T cell, and tissue damage amounts obtained from fifty one-year-long simulations, run for varying daily doses of pritelivir, are shown in figure 4.4. Median, rather than average, values are presented due to the highly skewed nature of the data during lesion events. This skew is caused by the large number of model reaction events that occur during the small time window of infection outbreaks. As pritelivir dosage increases, the median number of HSV-2 virions, CD4+ T cells, and amount of tissue damage decreases accordingly.

4.2. Pritelivir's Impact on HIV-1 Infection Probability

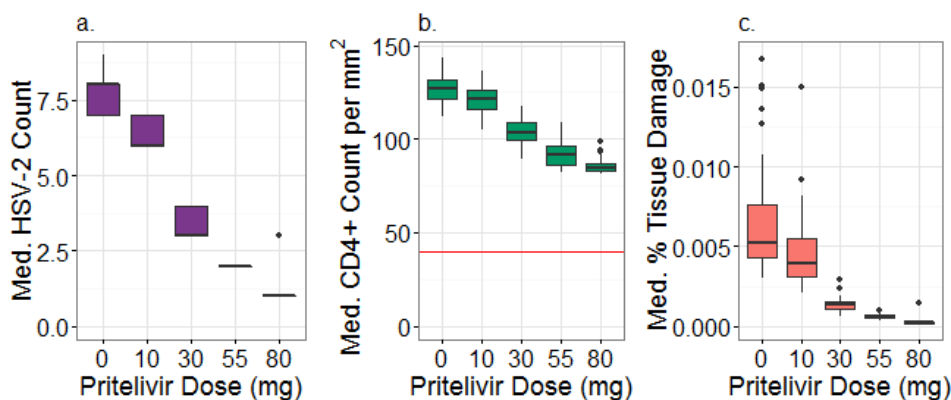


Figure 4.4: Median HSV-2 counts (a.), median CD4+ T cell counts per mm² (b.), and median percent of tissue damage (c.) for simulations run at five daily doses of pritelivir. The red horizontal line in b. shows the number of CD4+ T cells in healthy individuals (40 cells/mm²). All three values decrease as pritelivir dose increases; however, CD4+ T cell count remains the most stable.

In patients not receiving pritelivir, median HSV-2 viral loads ranged from 7-9 virions, and median tissue damage ranged from 0.003-0.017%. At doses of 80 mg/day, median HSV-2 counts in the simulation region were reduced 7.4 fold to between 1 and 3 virions, and tissue damage in the region was reduced 24.6 fold to approximately 0.0001% the simulation region. These results are confirmation that the symptoms associated with the HSV-2 infection have been greatly reduced as a result of antiviral use. Specifically, if we consider equation 4.4, the amount of median tissue damage at a pritelivir dose of 80 mg/day contributes only an additional 0.00000275% to the risk of HIV-1 contraction. Considering the background risk of HIV-1 is 0.005%, this increase can be considered negligible and indicates that at high doses of antiviral drugs CD4+ T cell counts become the greatest determinant of HIV-1 infection probability.

As depicted in figure 4.4, CD4+ T cell count appears the most stable infection characteristic as pritelivir dose increases. Between doses of 0 and 80 mg/day of pritelivir, median CD4+ T cell count only decreased by 1.5 fold and remained more than double the count seen in healthy tissue [48]. While the effects of lesions may become negligible, the maintenance of high CD4+ T cell counts may hinder the reduction of HIV-1 infection probability.

These trends are also apparent in figure 4.5 where median percent risks of HIV-1 contraction per coital act in one simulation region are shown for

4.2. Pritelivir's Impact on HIV-1 Infection Probability

varying doses of pritelivir. These values were obtained by inserting the median values of CD4+ T cells per mm^2 and median percents of tissue damage into equation 4.4. Similar to the 1.5 fold decrease seen across CD4+ T cells, the risk of HIV-1 infection shows a 1.8 fold decrease between doses of 0 and 80 mg/day of pritelivir. These results may help to explain why studies have not detected a significant decrease in HIV-1 infection probability in patients receiving HSV-2 antivirals [8, 46]. Even at a dosage of 80 mg/day, the median risk of HIV-1 for each of the 50 year long simulations remained 5.7-7.6 times larger than the 0.005% background risk of HIV-1 infection per (uninfected) simulation site that was calculated earlier. This result indicates that none of the pritelivir doses examined here are able to return the HSV-2 infected tissue to a fully healthy state.

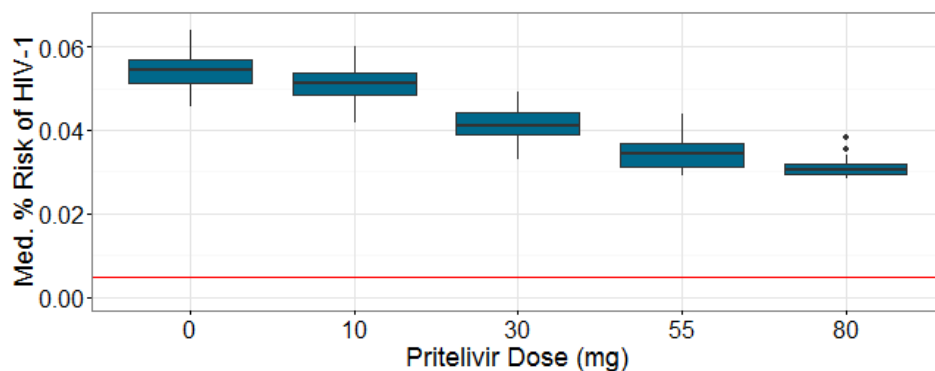


Figure 4.5: Median CD4+ T cell counts per mm^2 and median percent of tissue damage from model simulations describing the effects of varying doses of pritelivir were used to calculate the median risk of HIV-1 contraction in a simulation region per coital act. Risk of HIV-1 decreases with increases in pritelivir dose; however, risk remains well above that seen in healthy tissue, marked by the horizontal red line (0.005% per coital act).

While median HIV-1 infection probability shows a general decline as pritelivir dose increases, high variability in HIV-1 infection probability occurs throughout the course of a simulation. Figure 4.6 shows the changing risk of HIV-1 infection throughout the course of a year for varying doses of pritelivir. Spikes in infection probability occur during times of lesion development, showing up to a 60 fold increase. These spikes appear to occur at every dose. This observation serves as a clear indication that while patients on doses of pritelivir have a lower median risk, the current state of their

4.2. Pritelivir's Impact on HIV-1 Infection Probability

HSV-2 infection remains an important factor in their risk of contracting HIV-1.

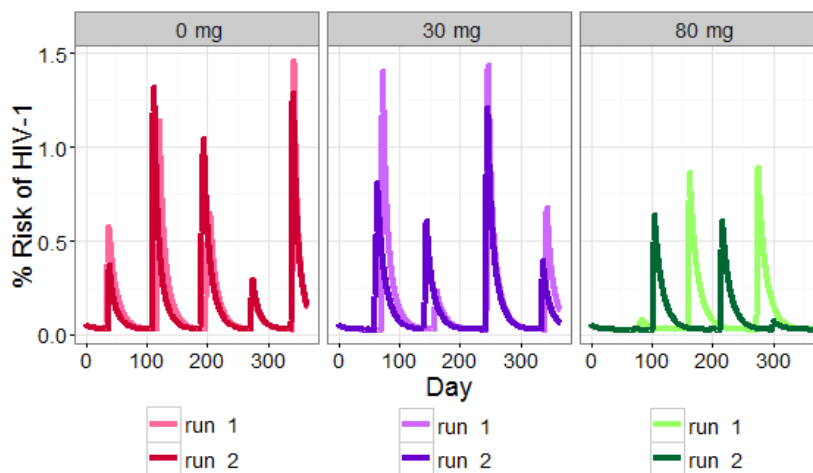


Figure 4.6: Changing risk of HIV-1 over time. For daily pritelivir doses of 0 mg, 30 mg, and 80 mg, two randomly chosen year-long simulations of the model were used to display the changes in HIV-1 infection risk over time. At every recorded time point, CD4+ T cell count and tissue damage were used to calculate the risk of HIV-1 using equation 4.4. For all doses, HIV-1 risk shows great variability over time.

4.2.1 HIV-1 Infection Probability for the Entire Genital Region

The simulations performed up to this point give a prediction of the probability of HIV-1 infection at one 4 cm^2 patch of genital epithelium. It may be more informative, however, to know the probability of HIV-1 infection per sexual act for the entire genital mucosa, as these values could be more easily compared to those recorded in the literature [6, 30, 32, 47]. This conversion of probabilities proves difficult as we cannot be sure at which stage of lesional development every patch of skin is experiencing, whether all patches of skin are chronically infected with HSV-2, or whether all patches of skin are exposed to the HIV-1 virus during a sexual act. To form some approximation, I looked at different states the estimated 88 cm^2 of the vagina may be experiencing in a chronically HSV-2 infected individual. I assumed that every 4 cm^2 patch, corresponding with one simulation region, could be experiencing a peak lesion event, some other chronic HSV-2 infected state,

4.2. Pritelivir's Impact on HIV-1 Infection Probability

or be unaffected by the HSV-2 virus and be considered healthy. I calculated the overall probability of HIV-1 infection for the entire vaginal region ($\text{Prob}_{inf,vag}$) using the following formula.

$$\text{Prob}_{inf,vag} = 1 - (1 - max)^a(1 - med)^b(1 - healthy)^c \quad (4.5)$$

Here, a is the number of 4 cm² epithelial patches that are experiencing a peak lesion, b is the number of 4 cm² epithelial patches that are experiencing some other state of lesion development, and c is the number of 4 cm² epithelial patches that are unaffected by the HSV-2 infection and can be considered healthy. Note that $a + b + c = 22$ as each patch is 4 cm² and the total area of the vagina is 88 cm².

For each dose of pritelivir, the probability of HIV-1 in a simulation site experiencing a peak lesion, termed max in equation 4.5, was defined as the average of the 95th percentile probabilities of infection for all fifty, one-year simulations run at that dose. Similarly, the average of the median probabilities of infection for each drug dose were used to represent the risk of HIV-1 infection in a region of HSV-2 infected tissue not experiencing a peak lesion event, termed med in equation 4.5. The probability of HIV-1 infection in a simulation region assumed to be healthy, termed $healthy$ in equation 4.5, was set to 0.00005, as found earlier in Chapter 3.

This formula assumes that infection at any site is independent of infection at other sites, and calculates the probability HIV-1 infection is established somewhere in the 22 patches. It also assumes all sites are exposed to HIV-1, and the concentration of HIV-1 virus is uniformly distributed across the vaginal tissue.

Results from these calculations for doses of 0 mg/day, 30 mg/day, and 80 mg/day of pritelivir are shown in figure 4.7. For an individual with all healthy tissue, the probability of HIV-1 infection is 0.11% per sexual act, matching with those values found in the literature [6, 30, 32, 47]. When an individual is not receiving treatment, every peak lesion adds an additional 0.8% to the risk of contracting HIV-1, and every 4 cm² patch of epithelial tissue that is experiencing some other state of HSV-2 infection adds an additional 0.05% to the risk of contracting HIV-1. If patients receive 30 mg/day of pritelivir, the risk of contracting HIV-1 in any of the vaginal tissue exposed shows a 1.11-1.32 fold decrease compared to the no treatment scenario depending on the tissue composition compared. This decrease may or may not be large enough to be captured in clinical studies. More promising, however, is the decrease in HIV-1 contraction risk with a dose of 80 mg/day of pritelivir, causing a 1.3-1.78 fold decrease in risk compared to the no treatment scenario.

4.2. *Pritelivir's Impact on HIV-1 Infection Probability*

When examining these overall risks of HIV-1 infection, another important aspect to consider is the likelihood of each tissue profile presented in figure 4.7. Since most HSV-2 positive patients spend the majority of their time with no symptomatic lesions, the top rows of these heatmaps are likely the best representation of the HIV-1 contraction risks most commonly faced by HSV-2 infected patients. Furthermore, HSV-2 lesions often re-occur in similar tissue regions, indicating that not the entire genital region should be considered chronically infected, further limiting the realistic tissue profile to the top left corner of these heatmaps. Other tissue profiles represent the per-coital HIV-1 risks that patients with more severe HSV-2 infections may experience. These more severe cases also become less likely as the dose of pritelivir increases and the occurrence of multiple genital lesions at one time becomes rare.

In patients not receiving antivirals, studies have recorded HIV-1 infection risk to be 2-3 times higher in HSV-2 asymptomatic, compared to healthy, patients and 7 times higher if lesions are present [3, 14]. These risks appear to match with those presented here when considering the most common tissue profiles.

4.2. Pritelivir's Impact on HIV-1 Infection Probability

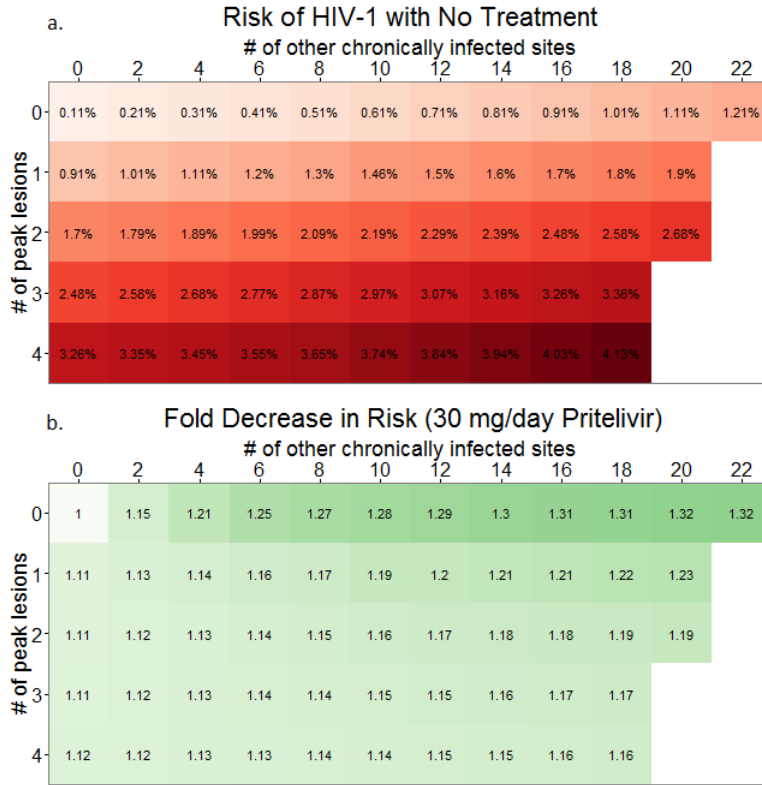


Figure 4.7: Probability of HIV-1 infection in vaginal tissue of an HSV-2 positive female, per coital act with a chronically HIV-1 infected male. With a vaginal surface area of 88 cm^2 , I assume the vaginal tissue can be represented by twenty-two 4 cm^2 simulation regions experiencing varying severities of HSV-2 infection. In a., the probability of HIV-1 infection in untreated individuals is shown. The top left grid square of the matrix represents the probability of HIV-1 infection given that all twenty-two tissue simulation regions in the vagina are healthy. Moving down the vertical axis, infection probability increases as sites of healthy tissue are replaced with severe lesions. Moving across the horizontal axis, healthy tissue becomes replaced with tissue experiencing median HSV-2 infection behaviour, also leading to an increase in HIV-1 infection probability, but to a lesser degree. For each examined tissue profile, heatmaps b. and c. show by what fold HIV-1 infection risk is predicted to decrease in patients receiving 30 mg and 80 mg of pritelivir a day respectively, compared to untreated patients.

4.2. Pritelivir's Impact on HIV-1 Infection Probability

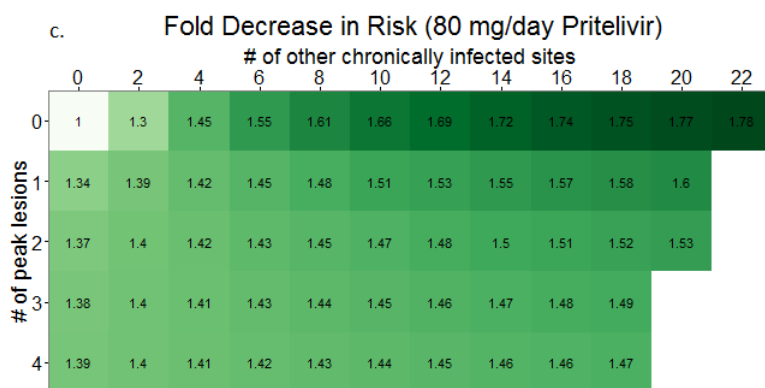


Figure 4.7 cont'd

Chapter 5

Conclusion

As the development of a trusted vaccination for HIV-1 may be far off, other strategies for controlling the spread of HIV-1 are important to develop and understand. With up to 60% of HIV-1 cases being attributed to previously established HSV-2 infections [14], it is important to see HSV-2 treatment as a way of controlling HIV-1 spread.

By developing a spatial stochastic model to describe the dynamics of chronic HSV-2 infections in the genital mucosa, I determined how HIV-1 infection probability can be expressed as a function of an individual's current HSV-2 infection state. With a particular focus on the newly developed HSV-2 antiviral drug pritelivir, I showed that doses currently being used in clinical trials should lower the risk of contracting HIV-1 by decreasing the frequency and severity of HSV-2 lesions that serve as entry points, and the number of CD4+ T cells in the genital mucosa that serve as target cells for HIV-1 virions. While the risk of contracting HIV-1 as a chronic HSV-2 infected individual receiving pritelivir still remains well above the risk faced by healthy, uninfected individuals, here I estimate that receiving 80 mg/day of pritelivir should cause a 1.3-1.78 fold decrease in the risk of contracting HIV-1 per coital act.

While theory has long predicted that such a decrease should result from HSV-2 antiviral drugs, clinical studies have failed to detect the effect of HSV-2 antivirals on the reduction of HIV-1 infection probability [18, 46]. Numerous reasons may explain this disconnect between theory and data, the first related to the CD4+ T cell counts in the studies' participants. In patients receiving HSV-2 antivirals, the mathematical model presented here predicts that CD4+ T cell counts in the genital mucosa become the greatest determinant in HIV-1 infection risk. Lowering CD4+ T cell count in the genital mucosa is essential to HIV-1 risk reduction. HSV-2 infection, however, may not be the only factor controlling CD4+ T cell counts in the genital mucosa. In clinical studies observing the effect of HSV-2 antivirals on HIV-1 infection probability, many participants were coinfecting with other STIs which were not controlled for [18, 46]. Non-ulcerative STIs can increase CD4+ T cell levels to twice those seen in healthy tissue [13]. Even if

participants were receiving HSV-2 antivirals, these extra CD4+ T cells due to other STIs may have kept CD4+ T cell counts too high for significant reductions in HIV-1 infection risk to occur.

Another potential reason why differences in HIV-1 risk were not captured with and without the use of HSV-2 antivirals in clinical studies may be due to sample sizes in the studies being too small. From the analysis presented here, the per-coital risk of contracting HIV-1 in chronically infected HSV-2 positive individuals remains very low, likely below 1.5%. While my analysis assumed partners were exposed to HIV-1 through unprotected sex, condom use in the clinical studies was encouraged [18, 46], likely bringing risks even lower and making them difficult to capture without a large sample size. Even more difficult may be capturing the difference in infection probability between the treated and untreated scenarios.

Differences in when, and how often, individuals from the control and treatment groups were having sex may have also helped mask HIV-1 risk differences in clinical studies. While individuals receiving antivirals generally have less severe lesions, they may have more small, undetectable microlesions which cause a flare in CD4+ T cell number and damaged skin that allows easier entry for the HIV-1 virus. While individuals may avoid sex when they have major, visible lesions, less caution may be taken during these other vulnerable times. This behaviour could potentially bring HIV-1 risks in the treated study participants closer to those seen in the untreated study participants.

Another more worrying reason of why antiviral drugs were not shown to reduce HIV-1 contraction risk in clinical studies may be due to short drug half lives. In the model presented here, antiviral drug decay was not considered. Previous mathematical models of HSV-2 infection, however, have included the effects of antiviral drug decay and show that when drug concentrations reach sub-therapeutic levels, rapid HSV-2 breakouts can occur, preventing full control of the infection [37]. The clinical studies aimed at detecting the effects of HSV-2 antivirals on HIV-1 infection risk have used acyclovir as their study drug which unfortunately has a short half-life of 3-4 hours [18, 46]. Lack of HIV-1 risk reduction in patients on these drugs may be explained by frequent times of sub-therapeutic drug levels. Fortunately, pritelivir's half-life is estimated to be approximately 80 hours [37]. This longer half-life should reduce the effects of drug decay on HSV-2 infection breakouts and HIV-1 infection probability. Longer half-lives also allow modelling the effects of antivirals as constant throughout time to be a safer assumption.

While the model presented here did not include the effects of drug decay,

it did incorporate CD4+ T cell dynamics in the genital mucosa, something which is novel to mathematical models describing HSV-2 infection. Unfortunately, their influence on the clearance of HSV-2 remained passive as not enough information is currently available to accurately predict their direct effects. By showing how essential CD4+ T cell numbers are to HIV-1 infection probabilities, this hopefully sparks more interest in studying their role and dynamics in herpes infections. It also may lead the way for more mathematical modelling of the synergy between HSV-2 and HIV-1 from the immunological perspective.

In conclusion, these results bring further insight to the mechanistic behaviour of herpes lesion development in the genital mucosa, the synergy between HSV-2 and HIV-1 infections, and provide support for HSV-2 antivirals being an effective way of controlling HIV-1 infection risk in patients with chronic HSV-2 infections. This study also helps inform clinicians in determining appropriate drug doses to see significant results in HIV-1 risk reduction. While clinical studies have been performed to examine the effects of pritelivir on HSV-2 infection alone, none have yet examined its effect of HIV-1 infection spread. The results presented here predict positive outcomes for such a study, and support further consideration of HSV-2 antivirals serving as a viable way to decrease probabilities of HIV-1 contraction. Furthermore, the modelling framework laid out here to examine the spatial development of lesions in the genital epithelium could potentially be expanded to mathematical studies of other skin abnormalities, building on our knowledge on tissue-resident immune cells and their interactions with invading pathogens.

Bibliography

- [1] G. Andrei, A. Lisco, C. Vanpouille, A. Introini, E. Balestra, J. van den Oord, T. Cihlar, C.-F. Perno, R. Snoeck, L. Margolis, and J. Balzarini. Topical tenofovir, a microbicide effective against HIV, inhibits herpes simplex virus-2 replication. *Cell Host & Microbe*, 10(4):379–389, 2011.
- [2] S. Ariotti, J. B. Beltman, G. Chodaczek, M. E. Hoekstra, A. E. van Beek, R. Gomez-Eerland, L. Ritsma, J. van Rheenen, A. F. Marea, T. Zal, R. J. de Boer, J. B. Haanen, and T. N. Schumacher. Tissue-resident memory CD8+ T cells continuously patrol skin epithelia to quickly recognize local antigen. *Proceedings of the National Academy of Sciences of the United States of America*, 109(48):19739–19744, 2012.
- [3] R. V. Barnabas and C. Celum. Infectious co-factors in HIV-1 transmission herpes simplex virus type-2 and HIV-1: new insights and interventions. *Current HIV Research*, 10(3):228–237, 2012.
- [4] C. Beauchemin. *Spatiotemporal Modelling of Viral Infection Dynamics*. PhD thesis, University of Alberta, Edmonton Alberta Canada, 2005.
- [5] C. Beauchemin, S. Forrest, and F. Koster. Modeling influenza viral dynamics in tissue. In *Proceedings of the Fifth International Conference on Artificial Immune Systems, ICARIS*, pages 23–36. Springer Verlag Berlin Heidelberg, 2006.
- [6] M. C. Boily, R. F. Baggaley, L. Wang, B. Masse, R. G. White, R. J. Hayes, and M. Alary. Heterosexual risk of HIV-1 infection per sexual act: systematic review and meta-analysis of observational studies. *The Lancet.Infectious Diseases*, 9(2):118–129, 2009.
- [7] A. M. Carias, S. McCoombe, M. McRaven, M. Anderson, N. Galloway, N. Vandergrift, A. J. Fought, J. Lurain, M. Duplantis, R. S. Veazey, and T. J. Hope. Defining the interaction of HIV-1 with the mucosal barriers of the female reproductive tract. *Journal of Virology*, 87(21): 11388–11400, 2013.

- [8] C. Celum, A. Wald, J. Hughes, J. Sanchez, S. Reid, S. Delany-Moretlwe, F. Cowan, M. Casapia, A. Ortiz, J. Fuchs, S. Buchbinder, B. Koblin, S. Zwierski, S. Rose, J. Wang, L. Corey, and HPTN 039 Protocol Team. Effect of aciclovir on HIV-1 acquisition in herpes simplex virus 2 seropositive women and men who have sex with men: a randomised, double-blind, placebo-controlled trial. *Lancet (London, England)*, 371(9630):2109–2119, 2008.
- [9] T. Chan, N. G. Barra, A. J. Lee, and A. A. Ashkar. Innate and adaptive immunity against herpes simplex virus type 2 in the genital mucosa. *Journal of Reproductive Immunology*, 88(2):210–218, 2011.
- [10] J. Conway, B. Konrad, and D. Coombs. Stochastic analysis of pre- and postexposure prophylaxis against HIV infection. *SIAM Journal on Applied Mathematics*, 73(2):904–928, 2013.
- [11] V. Dhankani, J. N. Kutz, and J. T. Schiffer. Herpes simplex virus-2 genital tract shedding is not predictable over months or years in infected persons. *PLoS Computational Biology*, 10(11):e1003922, 2014.
- [12] J. Elf and M. Ehrenberg. Spontaneous separation of bi-stable biochemical systems into spatial domains of opposite phases. *Systems Biology*, 1(2):230–236, 2004.
- [13] D. T. Fleming and J. N. Wasserheit. From epidemiological synergy to public health policy and practice: the contribution of other sexually transmitted diseases to sexual transmission of HIV infection. *Sexually Transmitted Infections*, 75(1):3–17, 1999.
- [14] E. E. Freeman, H. A. Weiss, J. R. Glynn, P. L. Cross, J. A. Whitworth, and R. J. Hayes. Herpes simplex virus 2 infection increases HIV acquisition in men and women: systematic review and meta-analysis of longitudinal studies. *AIDS (London, England)*, 20(1):73–83, 2006.
- [15] V. V. Ganusov and R. J. De Boer. Estimating in vivo death rates of targets due to CD8 T-cell-mediated killing. *Journal of Virology*, 82(23):11749–11757, 2008.
- [16] G. J. Goodhill. Diffusion in axon guidance. *The European Journal of Neuroscience*, 9(7):1414–1421, 1997.
- [17] R. Gupta, A. Wald, E. Krantz, S. Selke, T. Warren, M. Vargas-Cortes, G. Miller, and L. Corey. Valacyclovir and acyclovir for suppression of

- shedding of herpes simplex virus in the genital tract. *The Journal of Infectious Diseases*, 190(8):1374–1381, 2004.
- [18] A. T. Haase. Targeting early infection to prevent HIV-1 mucosal transmission. *Nature*, 464(7286):217–223, 2010.
- [19] F. Hladik and M. J. McElrath. Setting the stage: host invasion by HIV. *Nature Reviews Immunology*, 8(6):447–457, 2008.
- [20] J. E. Horbul, S. C. Schmechel, B. R. Miller, S. A. Rice, and P. J. Southern. Herpes simplex virus-induced epithelial damage and susceptibility to human immunodeficiency virus type 1 infection in human cervical organ culture. *PloS One*, 6(7):e22638, 2011.
- [21] A. Jansson, M. Harlen, S. Karlsson, P. Nilsson, and M. Cooley. 3D computation modelling of the influence of cytokine secretion on Th-cell development suggests that negative selection (inhibition of Th1 cells) is more effective than positive selection by IL-4 for Th2 cell dominance. *Immunology and Cell Biology*, 85(3):189–196, 2007.
- [22] Y. C. Jiang, H. Feng, Y. C. Lin, and X. R. Guo. New strategies against drug resistance to herpes simplex virus. *International Journal of Oral Science*, 8:1–6, 2016.
- [23] A. J. Johnson, C. F. Chu, and G. N. Milligan. Effector CD4+ T-cell involvement in clearance of infectious herpes simplex virus type 1 from sensory ganglia and spinal cords. *Journal of Virology*, 82(19):9678–9688, 2008.
- [24] C. Johnston, J. Zhu, L. Jing, K. J. Laing, C. M. McClurkan, A. Klock, K. Diem, L. Jin, J. Stanaway, E. Tronstein, W. W. Kwok, M. L. Huang, S. Selke, Y. Fong, A. Magaret, D. M. Koelle, A. Wald, and L. Corey. Virologic and immunologic evidence of multifocal genital herpes simplex virus 2 infection. *Journal of Virology*, 88(9):4921–4931, 2014.
- [25] B. E. Lai, M. H. Henderson, J. J. Peters, D. K. Walmer, and D. F. Katz. Transport theory for HIV diffusion through in vivo distributions of topical microbicide gels. *Biophysical Journal*, 97(9):2379–2387, 2009.
- [26] K. J. Looker, A. S. Magaret, K. M. Turner, P. Vickerman, S. L. Gottlieb, and L. M. Newman. Global estimates of prevalent and incident herpes simplex virus type 2 infections in 2012. *PloS One*, 10(1):e114989, 2015.

- [27] W. Mok, T. Stylianopoulos, Y. Boucher, and R. K. Jain. Mathematical modeling of herpes simplex virus distribution in solid tumors: implications for cancer gene therapy. *Clinical Cancer Research*, 15(7): 2352–2360, 2009.
- [28] Y. Nakanishi, B. Lu, C. Gerard, and A. Iwasaki. CD8+ T lymphocyte mobilization to virus-infected tissue requires CD4+ T-cell help. *Nature*, 462(7272):510–513, 2009.
- [29] C. Noecker, K. Schaefer, K. Zaccheo, Y. Yang, J. Day, and V. V. Ganusov. Simple mathematical models do not accurately predict early SIV dynamics. *Viruses*, 7(3):1189–1217, 2015.
- [30] P. Patel, C. B. Borkowf, J. T. Brooks, A. Lasry, A. Lansky, and J. Mermin. Estimating per-act HIV transmission risk: a systematic review. *AIDS (London, England)*, 28(10):1509–1519, 2014.
- [31] J. E. Pearson, P. Krapivsky, and A. S. Perelson. Stochastic theory of early viral infection: continuous versus burst production of virions. *PLoS Computational Biology*, 7(2):e1001058, 2011.
- [32] S. D. Pinkerton. Probability of HIV transmission during acute infection in Rakai, Uganda. *AIDS and Behavior*, 12(5):677–684, 2008.
- [33] T. Schacker, A. J. Ryncarz, J. Goddard, K. Diem, M. Shaughnessy, and L. Corey. Frequent recovery of HIV-1 from genital herpes simplex virus lesions in HIV-1-infected men. *Jama*, 280(1):61–66, 1998.
- [34] J. T. Schiffer, L. Abu-Raddad, K. E. Mark, J. Zhu, S. Selke, A. Magaret, A. Wald, and L. Corey. Frequent release of low amounts of herpes simplex virus from neurons: results of a mathematical model. *Science Translational Medicine*, 1(7):7–16, 2009.
- [35] J. T. Schiffer, L. Abu-Raddad, K. E. Mark, J. Zhu, S. Selke, D. M. Koelle, A. Wald, and L. Corey. Mucosal host immune response predicts the severity and duration of herpes simplex virus-2 genital tract shedding episodes. *Proceedings of the National Academy of Sciences of the United States of America*, 107(44):18973–18978, 2010.
- [36] J. T. Schiffer, D. Swan, R. Al Sallaq, A. Magaret, C. Johnston, K. E. Mark, S. Selke, N. Ocbamichael, S. Kuntz, J. Zhu, B. Robinson, M. L. Huang, K. R. Jerome, A. Wald, and L. Corey. Rapid localized spread and immunologic containment define herpes simplex virus-2 reactivation in the human genital tract. *eLife*, 2:e00288, 2013.

- [37] J. T. Schiffer, D. A. Swan, A. Magaret, L. Corey, A. Wald, J. Ossig, H. Ruebsamen-Schaeff, S. Stoelben, B. Timmler, H. Zimmermann, M. R. Melhem, S. A. Van Wart, C. M. Rubino, and A. Birkmann. Mathematical modeling of herpes simplex virus-2 suppression with pritelivir predicts trial outcomes. *Science Translational Medicine*, 8(324):324ra15, 2016.
- [38] A. Simmons and D. C. Tschärke. Anti-CD8 impairs clearance of herpes simplex virus from the nervous system: implications for the fate of virally infected neurons. *The Journal of Experimental Medicine*, 175(5):1337–1344, 1992.
- [39] M. A. Stafford, L. Corey, Y. Cao, E. S. Daar, D. D. Ho, and A. S. Perelson. Modeling plasma virus concentration during primary HIV infection. *Journal of Theoretical Biology*, 203(3):285–301, 2000.
- [40] L. R. Stanberry, E. R. Kern, J. T. Richards, T. M. Abbott, and J. Overall, J. C. Genital herpes in guinea pigs: pathogenesis of the primary infection and description of recurrent disease. *The Journal of Infectious Diseases*, 146(3):397–404, 1982.
- [41] S. L. Swain, K. K. McKinstry, and T. M. Strutt. Expanding roles for CD4(+) T cells in immunity to viruses. *Nature Reviews.Immunology*, 12(2):136–148, 2012.
- [42] R. Turner, Z. Shehab, K. Osborne, and J. O. Hendley. Shedding and survival of herpes simplex virus from ‘fever blisters’. *Pediatrics*, 70(4):547–549, 1982.
- [43] A. Wald and K. Link. Risk of human immunodeficiency virus infection in herpes simplex virus type 2-seropositive persons: a meta-analysis. *The Journal of Infectious Diseases*, 185(1):45–52, 2002.
- [44] A. Wald, L. Corey, B. Timmler, A. Magaret, T. Warren, S. Tying, C. Johnston, J. Kriesel, K. Fife, L. Galitz, S. Stoelben, M. L. Huang, S. Selke, H. P. Stobernack, H. Ruebsamen-Schaeff, and A. Birkmann. Helicase-primase inhibitor pritelivir for HSV-2 infection. *The New England Journal of Medicine*, 370(3):201–210, 2014.
- [45] S. Wang, P. Hottz, M. Schechter, and L. Rong. Modeling the slow CD4+ T cell decline in HIV-infected individuals. *PLoS Computational Biology*, 11(12):e1004665, 2015.

- [46] D. Watson-Jones, H. A. Weiss, M. Rusizoka, J. Changalucha, K. Baisley, K. Mugeye, C. Tanton, D. Ross, D. Everett, T. Clayton, R. Balira, L. Knight, I. Hambleton, J. Le Goff, L. Belec, and R. Hayes. Effect of herpes simplex suppression on incidence of HIV among women in Tanzania. *New England Journal of Medicine*, 358(15):1560–1571, 2008. doi: 10.1056/NEJMoa0800260.
- [47] M. J. Wawer, R. H. Gray, N. K. Sewankambo, D. Serwadda, X. Li, O. Laeyendecker, N. Kiwanuka, G. Kigozi, M. Kiddugavu, T. Lutalo, F. Nalugoda, F. Wabwire-Mangen, M. P. Meehan, and T. C. Quinn. Rates of HIV-1 transmission per coital act, by stage of HIV-1 infection, in Rakai, Uganda. *The Journal of Infectious Diseases*, 191(9):1403–1409, 2005.
- [48] J. Zhu, F. Hladik, A. Woodward, A. Klock, T. Peng, C. Johnston, M. Remington, A. Magaret, D. M. Koelle, A. Wald, and L. Corey. Persistence of HIV-1 receptor-positive cells after HSV-2 reactivation is a potential mechanism for increased HIV-1 acquisition. *Nature Medicine*, 15(8):886–892, 2009.

Appendix A

Main Python Code for HSV-2 Infection Simulations

```
1 #LIBRARIES
2 import time
3 import re
4 import math
5 import numpy as np
6 from numpy import array
7 from numpy.random import uniform, multinomial, exponential,
   random
8 from numpy import arange, array, empty, zeros, log
9 import time
10 import multiprocessing
11
12 #TECHNICAL INFORMATION
13 #Size Dimensions
14 Dim= 2.0 #cm
15 x_box = 15
16 y_box = 15
17 h = Dim/x_box
18
19 #Run Time Specifications
20 S_max = 1
21 N_max =1
22 t_max = 120
23 recInterval = 0.01
24
25 #REACTIONS
26 #r0 = creation of healthy epithelial cells
27 #r1 = infection of healthy cell by an epithelial virus
28 #r2 = infection of a healthy cell by a neuronal virus
29 #r3 = death of infected epithelial cells
30 #r4 = clearance of infected epithelial cells by CD8
31 #r5 = production of more CD8s
32 #r6 = death of CD8s
33 #r7 = production of epithelial virus
34 #r8 = decay of epithelial virus
35 #r9 = decay of neuronal virus
```

Appendix A. Main Python Code for HSV-2 Infection Simulations

```

36 #r10 = release of virus from neuron – only occurs in the centre
    box
37 #r11 = diffusion of epithelial virus
38 #r12 = diffusion of neuronal virus
39 #r13 = diffusion of CD8
40 #r14 = diffusion of CD4
41 #r15 = diffusion of cytokines
42 #r16 = bringing in of more CD8 from borders
43 #r17 = bringing in of more CD4 from borders
44 #r18 = production of more CD4s
45 #r19 = death of CD4s
46 #r20 = flow in of more CD4s
47 #r21 = production of cytokines
48 #r22 = decay of cytokines
49
50 tmat = array([[1, -1, -1, 0, 0, 0, 0, 0, 0, 0, 0, 0, 0,
51               0, 0, 0, 0, 0, 0, 0, 0, 0, 0], #H
52               [0, 1, 1, -1, -1, 0, 0, 0, 0, 0, 0, 0, 0, 0,
53               0, 0, 0, 0, 0, 0, 0, 0, 0, 0], #I
54               [0, 0, 0, 0, 0, 0, 1, -1, 0, 0, 0, 0, 0, 0,
55               0, -1, 0, 0, 1, 0, 0, 0, 0, 0, 0], #E
56               [0, -1, 0, 0, 0, 0, 0, 0, 1, -1, 0, 0, -1,
57               0, 0, 0, 0, 0, 0, 0, 0, 0, 0], #Ve
58               [0, 0, -1, 0, 0, 0, 0, 0, 0, 0, -1, 1, 0,
59               -1, 0, 0, 0, 0, 0, 0, 0, 0, 0], #Vn
60               [0, 0, 0, 0, 0, 0, 0, 0, 0, 0, 0, 0, 0, 0,
61               0, 0, -1, 0, 0, 1, 1, -1, 1, 0, 0], #T
62               [0, 0, 0, 0, 0, 0, 0, 0, 0, 0, 0, 0, 0, 0,
63               0, 0, 0, -1, 0, 0, 0, 0, 0, 1, -1] #C
64           ])
65
66 def fcn(var1, var2, var3):
67     H = H_counter[var1, var2]
68     I = I_counter[var1, var2]
69     E = E_counter[var1, var2]
70     Ve = Ve_counter[var1, var2]
71     Vn = Vn_counter[var1, var2]
72     T = T_counter[var1, var2]
73     C = C_counter[var1, var2]
74     #determine how many exposed edges the chosen box has
75     edges = sum([var1==0, var1 == x_box - 1, var2==0, var2==y_box
76                 -1])
77     ra = zeros(23, dtype=float)
78     ra[0] = g*(H0-H)
79     ra[1] = beta*H*Ve
80     ra[2] = beta*H*Vn
81     ra[3] = a*I
82     ra[4] = f*I*E
83     ra[5] = C/(C+r3)*theta1*E

```

Appendix A. Main Python Code for HSV-2 Infection Simulations

```

83     ra[6] = delta*E
84     ra[7] = p*I
85     ra[8] = c*Ve
86     ra[9] = c*Vn
87     if var1==round(x_box/2,0) and var2==round(x_box/2,0):
88         ra[10] = phi
89     else:
90         ra[10] = 0
91     ra[11] = diff1*Ve
92     ra[12] = diff1*Vn
93     ra[13] = diff2*E
94     ra[14] = diff2*T
95     ra[15] = diff3*C
96     if edges>0:
97         ra[16] = edges*D_E
98         ra[17] = edges*D_T
99     else:
100        ra[16] = 0
101        ra[17] = 0
102    ra[18] = C/(C+r4)*theta2*T
103    ra[19] = d*T
104    ra[20] = Lambda
105    ra[21] = b*I
106    ra[22] = m*C
107
108    rate = ra.sum()
109    if var3==1:
110        if rate>0:
111            delta_t = -math.log(np.random.uniform(0,1,1))/rate
112        else:
113            delta_t = 1000000
114        return delta_t
115    elif var3==2:
116        event = np.random.multinomial(1,ra/rate)
117        return event
118
119    def diffusion(counter):
120        if id(counter)==id(C_counter) or id(counter) ==id(Ve_counter)
121            or id(counter) == id(Vn_counter):
122            event2 = np.random.multinomial(1,[0.25,0.25,0.25,0.25])
123        else:
124            Cneigh = zeros(4, dtype=float)
125            if X>0:
126                Cneigh[0] = C_counter[X-1,Y]
127            if X<x_box-1:
128                Cneigh[1] = C_counter[X+1,Y]
129            if Y>0:
130                Cneigh[2] = C_counter[X,Y-1]
131            if Y<y_box-1:

```

Appendix A. Main Python Code for HSV-2 Infection Simulations

```
131     Cneigh[3] = C_counter[X,Y+1]
132     Ctot = sum(Cneigh)
133     if Ctot>0:
134         event2 = np.random.multinomial(1, Cneigh/Ctot)
135     else:
136         event2 = np.random.multinomial(1, [0.25, 0.25, 0.25, 0.25])
137     if event2[0]==1 and X>0:
138         counter[X-1,Y]+=1
139         delta_t = fcn(X-1,Y,1)
140         t[X-1,Y] = t_counter+delta_t
141     elif event2[1]==1 and X<x_box-1:
142         counter[X+1,Y]+=1
143         delta_t = fcn(X+1,Y,1)
144         t[X+1,Y] = t_counter+delta_t
145     elif event2[2]==1 and Y>0:
146         counter[X,Y-1]+=1
147         delta_t = fcn(X,Y-1,1)
148         t[X,Y-1] = t_counter+delta_t
149     elif event2[3]==1 and Y<y_box-1:
150         counter[X,Y+1]+=1
151         delta_t = fcn(X,Y+1,1)
152         t[X,Y+1] = t_counter+delta_t
153
154
155 #INITIAL CONDITIONS
156 H = round(6024382/(x_box*y_box), 0)
157 I = 0
158 E = 60000
159 C = 0
160 Ve = 0
161 Vn = 0
162 T = 50000
163
164 #MODEL SPECIFICATIONS
165
166 #Parameters
167 g = 0.22
168 H0 = H
169 beta = 1*x_box*y_box*pow(10, -7)
170 a = 1.2
171 f = 0.01*x_box*y_box
172 r3 = 42.0/(x_box*y_box)
173 theta1 = 1.7
174 delta = 0.05
175 p = 7.05*pow(10, 3)
176 c = 8.8
177 phi = 50
178 m = 6.2
179 b = 24.8
```

Appendix A. Main Python Code for HSV-2 Infection Simulations

```

180 d = 0.07
181 theta2 = 1.4
182 r4 = 38.0/(x_box*y_box)
183 Lambda = 1900.0/(x_box*y_box)
184 omegav = 0.00072
185 omegae = 0.00072
186 omegac = 0.0245
187 diff1 = 4*omegav/pow(h,2)
188 diff2 = 4*omegae/pow(h,2)
189 diff3 = 4*omegac/pow(h,2)
190 #rates of diffusion from borders
191 D_E = omegae*E/(pow(h,2)*(x_box*y_box))
192 D_T = omegae*T/(pow(h,2)*(x_box*y_box))
193 #Counters
194 H_counter = np.zeros((x_box, y_box))
195 I_counter = np.zeros((x_box, y_box))
196 E_counter = np.zeros((x_box, y_box))
197 C_counter = np.zeros((x_box, y_box))
198 Ve_counter = np.zeros((x_box, y_box))
199 Vn_counter = np.zeros((x_box, y_box))
200 T_counter = np.zeros((x_box, y_box))
201 t_counter = 0
202 t = np.zeros((x_box, y_box))
203
204 #OTHER FUNCTIONS
205
206
207 def printing(fileName, counter, savetype, format):
208     with file(fileName, savetype) as fileshort:
209         np.savetxt(fileshort, counter, fmt=format)
210         fileshort.write('# New step\n')
211
212 #MODEL
213 N = 0
214 while (N<=N_max-1):
215     S = 0
216     H_counter[:, :] = H
217     I_counter[:, :] = I
218     XY_list = np.random.random_integers(x_box, size=(E,2.))-1
219     for i in range(0,E):
220         E_counter[XY_list[i,0], XY_list[i,1]] = E_counter[XY_list[i
221             ,0], XY_list[i,1]]+1
222     C_counter[:, :] = C
223     Ve_counter[:, :] = Ve
224     Vn_counter[:, :] = Vn
225     XY_list2 = np.random.random_integers(x_box, size=(T,2.))-1
226     for i in range(0,T):
227         T_counter[XY_list2[i,0], XY_list2[i,1]] = T_counter[XY_list2[
228             i,0], XY_list2[i,1]]+1

```

Appendix A. Main Python Code for HSV-2 Infection Simulations

```
227 t_counter = 0
228 t[:, :] = 0
229
230
231 while t_counter < t_max:
232     S += 1
233     if S == 1:
234         #Set up initial time queue
235         for i in range(0, x_box):
236             for j in range(0, y_box):
237                 delta_t = fcn(i, j, 1)
238                 t[i, j] = delta_t
239
240         #Select box for reaction to occur and update the t_counter
241         Hit = np.where(t == np.min(t))
242         Hit = np.asmatrix(Hit)
243         X = Hit[0]
244         Y = Hit[1]
245
246         if np.shape(Hit) != (2, 1):
247             X = Hit[0, 0]
248             Y = Hit[1, 0]
249             print 'True'
250         t_counter = t[X, Y]
251
252
253         #Choose an event to occur the selected box
254         event = fcn(X, Y, 2)
255         changes = tmat[:, event.nonzero()[0][0]]
256         #Update centre box
257         H_counter[X, Y] += changes[0]
258         I_counter[X, Y] += changes[1]
259         E_counter[X, Y] += changes[2]
260         Ve_counter[X, Y] += changes[3]
261         Vn_counter[X, Y] += changes[4]
262         T_counter[X, Y] += changes[5]
263         C_counter[X, Y] += changes[6]
264
265         #Update side boxes and time queue
266         if sum(event[11:16]) > 0:
267
268             if event[11] == 1:
269                 diffusion(Ve_counter)
270             elif event[12] == 1:
271                 diffusion(Vn_counter)
272             elif event[13] == 1:
273                 diffusion(E_counter)
274             elif event[14] == 1:
275                 diffusion(T_counter)
```

Appendix A. Main Python Code for HSV-2 Infection Simulations

```
276         elif event[15]==1:
277             diffusion(C_counter)
278
279 #Update time queue for central box
280 delta_t = fcn(X,Y,1)
281 t[X,Y] = t[X,Y]+delta_t
282
283 if S==1 and N == 0:
284     tpoint = t_counter
285     printing('H.mat.txt',H_counter,'w','%1.0f')
286     printing('I.mat.txt',I_counter,'w','%1.0f')
287     printing('E.mat.txt',E_counter,'w','%1.0f')
288     printing('C.mat.txt',C_counter,'w','%1.0f')
289     printing('V.mat.txt',Ve_counter+Vn_counter,'w','%1.0f')
290     printing('Tcell.mat.txt',T_counter,'w','%1.0f')
291     printing('t.mat.txt',t_counter,'w','%1.0e')
292
293 elif (S==1 and N!=0) or \
294 t_counter>=tpoint+recInterval:
295     tpoint = t_counter
296     printing('H.mat.txt',H_counter,'a','%1.0f')
297     printing('I.mat.txt',I_counter,'a','%1.0f')
298     printing('E.mat.txt',E_counter,'a','%1.0f')
299     printing('C.mat.txt',C_counter,'a','%1.0f')
300     printing('V.mat.txt',Ve_counter+Vn_counter,'a','%1.0f')
301     printing('Tcell.mat.txt',T_counter,'a','%1.0f')
302     printing('t.mat.txt',t_counter,'a','%1.0e')
303
304 N+=1
```